Manuscript title

The scaffold protein IQGAP1 links heat-induced stress signals to alternative splicing regulation in gastric cancer cells

Andrada Birladeanu[1,*], Malgorzata Rogalska[2,3,*], Myrto Potiri[1,*], Vasiliki Papadaki[1], Margarita Andreadou[1], Dimitris L. Kontoyiannis[1,4], Joe D. Lewis[5], Zoi Erpapazoglou[1], Panagiota Kafasla[1,6]

[1]Institute for Fundamental Biomedical Research, B.S.R.C. "Alexander Fleming", 34 Fleming st. 16672 Vari, Athens, Greece

[2]Centre for Genomic Regulation (CRG), The Barcelona Institute of Science and Technology, Dr Aiguader 88, Barcelona 08003, Spain

[3]Universitat Pompeu Fabra (UPF), Barcelona 08003, Spain

[4]Department of Biology, Aristotle University of Thessaloniki, Greece

[5]European Molecular Biology Laboratory, 69117 Heidelberg, Germany

[6]To whom correspondence should be addressed: Email: kafasla@fleming.gr

[*]These authors contributed equally to this work

Conflict of Interest: The authors declare no conflict of interest.

ABSTRACT

In response to oncogenic signals, Alternative Splicing (AS) regulators such as SR and hnRNP proteins show altered expression levels, subnuclear distribution and/or post-translational modification status, but the link between signals and these changes remains unknown. Here, we report that a cytosolic scaffold protein, IQGAP1, performs this task in response to heat-induced signals. We show that in gastric cancer cells, a nuclear pool of IQGAP1 acts as a tethering module for a group of spliceosome components, including hnRNPM, a splicing factor critical for the response of the spliceosome to heat-shock. IQGAP1 controls hnRNPM's sumoylation, subnuclear localization and the relevant response of the AS machinery to heat-induced stress. Genome-wide analyses reveal that IQGAP1 and hnRNPM co-regulate the AS of a cell cycle-related RNA regulon in gastric cancer cells, thus favouring the accelerated proliferation phenotype of gastric cancer cells. Overall, we reveal a missing link between stress signals and AS regulation.

INTRODUCTION

In humans, more than 95% of multi-exonic genes are potentially alternatively spliced (1,2). The importance of accurate AS in health and disease, including cancer, has been well documented (3–7). Most data linking AS, signaling and cancer comes from cases where localization, expression, or post-translational modifications of splicing factors like SR proteins or hnRNPs are altered (7). In the cytoplasm, signalling integrators such as the scaffold proteins spatially organise signalling enzymes and guide the flow of molecular information (8). In the nucleus, a few cases have been identified, involved in nuclear protein quality control and transcriptional regulation (9,10). However, information is missing on how signals reach the splicing machinery and alter splicing outcome.

In our search for signal transducers to the splicing complexes, we came across the scaffold protein IQGAP1 (IQ-Motif Containing GTPase Activating Protein 1) in LC-MS/MS data of

hnRNP complexes in mouse and human cell lines. IQGAP1 has been previously detected as a component of distinct spliceosomal complexes by LC-MS/MS analyses (11,12).

IQGAP1 is primarily cytoplasmic, acting as a signal integrator in many pathways. Increasing evidence reveals nuclear functions of IQGAP1. IQGAP1 accumulates in the nucleus at the G1/S phase of the cell cycle (13). It interacts with and influences the function of a variety of transcription factors (14,15). IQGAP1 is important for induction of nuclear F-actin in response to replication stress (16). With *IQGAP1* mRNA being overexpressed in many malignant cell types, the protein seems to regulate cancer growth and metastatic potential (17–20). Moreover, aged mice lacking IQGAP1 develop gastric hyperplasia suggesting an important *in vivo* role for IQGAP1 in maintaining the gastric epithelium (21).

Here, we present conclusive evidence on the participation of IQGAP1 in nuclear ribonucleoprotein complexes (RNPs) in gastric cancer, a cancer type characterized by significantly high incidence of AS changes (4,6). We show that IQGAP1 controls the subcellular distribution of AS regulatory proteins and is necessary for the response of the splicing machinery to heat-induced signals in gastric cancer cells. Focusing on the interaction of IQGAP1 with hnRNPM, a known splicing regulator (22,23) that responds to heat-shock by moving away from spliceosomal complexes (12,22) and is sumoylated by SUMO2 in response to heat stress (24–27), we show that IQGAP1 regulates the subnuclear distribution and post-translational status of hnRNPM. We finally show that hnRNPM-IQGAP1 support tumour promoting AS of cell cycle regulators, such as the substrate recognizing subunit of the anaphase promoting complex/cyclosome (APC/C), ANAPC10. In the absence of hnRNPM-IQGAP1 RNPs, cell cycle progression and tumour growth are halted, making the two proteins and their interaction an interesting cancer drug target.

MATERIAL AND METHODS

Source of reagents, cell lines, cell culture conditions, and detailed experimental procedures for standard methods (e.g. transfections, subcellular Fractionation, immunoprecipitation,

knockout generation, splicing assays, microscopy techniques and quantitation, immunostaining) are described in the Supplementary Material and Methods section.

Cell cultures

The human STAD cell lines AGS, KATOIII, MKN45 and NUGC4 were used. When indicated, cells were treated with the sumoylation inhibitor III 2-D08 (Millipore, Cat# 505156) at 100 μM for 12 h.

Mass spectrometry and Proteomics analysis

Anti-IQGAP1 immunoprecipitation samples were processed in collaboration with the Core Proteomics Facility at EMBL Heidelberg. See Supplementary Materials and Methods.

RNA-seq analysis

AS was analysed by using VAST-TOOLS v2.2.2 (29) and expressed as changes in percent-spliced-in values (ΔPSI). To generate RNA maps, we used the rna_maps function (30), using sliding windows of 15 nucleotides as described in Supplementary Materials and Methods.

Quantification and Statistical Analysis

Data were analysed using GraphPad Prism 7 software (GraphPad Software). Student's t test (comparisons between two groups), one-way ANOVA were used as indicated in the legends. $p < 0.05$ was considered statistically significant.

ACCESSION NUMBERS

The mass spectrometry proteomics data have been deposited to the ProteomeXchange Consortium via the PRIDE[69] partner repository with the dataset identifier PXD017842.

RNA-seq data have been deposited in GEO: GSE146283.

RESULTS

IQGAP1 expression levels are significantly increased in gastric cancer cells

Immunofluorescent analysis of the IQGAP1 protein levels on commercial gastric tissue microarrays revealed increased immunostaining in tumour as compared to normal tissue, especially in adenocarcinoma and signet-ring cell carcinoma samples (Figs. 1A-B, S1A). This finding agrees with TCGA data analyses that indicate significantly increased expression of *IQGAP1* mRNA in stomach adenocarcinoma (STAD) and esophagogastric cancers (STES) vs normal tissue (Fig. 1C). Furthermore, high IQGAP1 expression in STES and STAD tumours predicts low survival probability for patients (Fig. S1B-C).

Assaying IQGAP1 protein levels in a number of STAD cell lines identified cell lines with lower (MKN45, AGS) or higher (NUGC4, KATOIII) levels of IQGAP1 (Fig. 1D). Two STAD cell lines with significantly different IQGAP1 levels were used for further studies: NUGC4, a gastric signet-ring cell adenocarcinoma cell line, derived from paragastric lymph node metastasis and MKN45, a gastric adenocarcinoma cell line, derived from a liver metastatic site.

Nuclear IQGAP1 is a component of RNPs involved in splicing regulation

Nuclear IQGAP1 can be detected in a small fraction of untreated cells (13). Similarly, we detected nuclear IQGAP1 in both STAD cell lines, the high-IQGAP1, NUGC4 and the low-IQGAP1, MKN45, using immunofluorescence and confocal imaging (Fig. 2A). Nuclear IQGAP1 was also detected in a fraction of cells in cancer tissue samples of the microarray (Fig. 1A).

To assess the role of nuclear IQGAP1 we identified its interacting partners using anti-IQGAP1 immunoprecipitation from nuclear extracts derived from the high-IQGAP1 cell line followed by LC-MS/MS (Table S1). The extract preparations used in our assays are enriched for the majority of hnRNPs (31,32) (e.g. A2B1, K, M), other nuclear speckle components like

SRSF1, and nuclear matrix proteins like SAFB and MATRIN3, but not histones such as H3, which are present mainly in the insoluble nuclear material (Fig. S2A-B).

GO-term enrichment analysis of the nuclear IQGAP1 co-precipitated proteins showed a significant enrichment in biological processes related to splicing regulation (Fig. S2C). The derived IQGAP1 interaction network revealed that IQGAP1 interacts with the majority of hnRNPs, a large number of spliceosome components (mainly of U2, U5snRNPs) and RNA-modifying enzymes (Fig. 2B). The interactions between IQGAP1 and selected hnRNPs, spliceosome components and RNA processing factors (33) were further validated in both STAD cell lines in use (Figs. 2C, S2D). The interactions of IQGAP1 with hnRNPs A1, A2B1 are RNA-dependent, whereas a subset of hnRNPs L and C1/C2 can interact with IQGAP1 in the absence of RNA. The interaction between IQGAP1 and hnRNPM is different between the two cell lines: partly RNA-dependent in the low-IQGAP1, but RNA-independent in the high-IQGAP1 (Fig. 2C). These data suggest a role for the nuclear IQGAP1 in splicing regulation.

IQGAP1 participates in AS regulation in gastric cancer cell lines

To further study the role of nuclear IQGAP1 in gastric cancer cells we knocked-out (KO) successfully *IQGAP1* in both STAD cell lines using a CRISPR-Cas9 approach, without affecting significantly hnRNPM protein levels (Figs. 3A, S3A).

To assess the functional involvement of IQGAP1 in splicing we used the three-exon minigene splicing reporters DUP51M1 and DUP50M1. During splicing, hnRNPM binds exon 2 of the respective pre-mRNAs and prevents its inclusion (28). Transfection of the parental and the derived KO cell lines with the reporter plasmids and subsequent RT-PCR analyses revealed different splicing patterns of the reporter: increased exon 2 inclusion in the high-IQGAP1 cells (NUGC4) (73%, Fig. S3A) compared to the low-IQGAP1 ones (MKN45) (31%, Fig. 3A). Downregulation of *IQGAP1* resulted in increased exon 2 inclusion in both KO cell

147 lines, compared to the parental cells (Figs. 3A, S3A-B). This change was more apparent in
148 the low-IQGAP1 cell line (~2-fold increase of exon 2 inclusion in *IQGAP1*^{KO} cells compared
149 to the parental ones). Co-transfection of MKN45-*IQGAP1*^{KO} cells with two different amounts
150 of a Myc-IQGAP1 expressing plasmid (34) which produced a protein localized similarly to
151 endogenous IQGAP1 (Fig. S3C), restored the AS pattern of the reporter to levels similar to
152 the MKN45 ones (Fig. 3A-B), confirming the direct involvement of IQGAP1 in the AS of the
153 reporter.

154 To gain further insight on the importance of IQGAP1 in AS regulation in STAD, we profiled
155 AS pattern changes between the low-IQGAP1 cell line, which is more responsive to IQGAP1
156 depletion, and the respective *IQGAP1*^{KO} cells by RNA-seq. A number of significantly altered
157 AS events were detected (Table S2A), more than 50% of which were alternative exons (Fig.
158 3C), with similar distribution of ΔPsi values for the downregulated and upregulated events
159 (where [Psi] is the Percent Spliced In, i.e. the ratio between reads including or excluding
160 alternative exons) (Fig. S3D).

161 GO-term enrichment analysis of the affected genes yielded significant enrichment of the
162 biological processes of cell cycle (GO:0007049, P: 3.75E-04) and cell division (GO:0051301,
163 P: 3.33E-04) (Fig. 3D, Table S2B). Similarly, GO-term enrichment analysis of the
164 differentially expressed genes upon *IQGAP1*^{KO} revealed significant enrichment of cell cycle-
165 related biological processes (Fig. S3E, Table S2C). However, only 5 genes were
166 differentially expressed and differentially spliced (Table S2D), indicating that IQGAP1's
167 regulation of cell cycle at the level of AS is distinct from that at the levels of transcription or
168 mRNA stability (35,36).

169 To focus on the role of IQGAP1 in AS we validated selected events by RT-PCR analyses
170 (Figs. 3E-F, S3F), chosen based on the following criteria: 1) high difference in Psi (ΔPsi)
171 between the KO and the parental cell lines, 2) involvement of the respective proteins in the
172 cell cycle, 3) characterization of the event as SOK (Super okay), or OK (okay) based on the

quality scores acquired during the analysis (29). 12 out of 19 AS events (63%) were validated (Figs. 3E-F, S3F, Table S3).

Following validation, we searched the sequences surrounding the alternative exons for enrichment of binding motifs of IQGAP1-interacting splicing factors (Fig. 2). Such analyses revealed a significant enrichment of hnRNPM binding motifs downstream of 25% of the downregulated exons (Fig. 3G). Enrichment of the binding motifs of other IQGAP1-interacting splicing factors was observed in smaller percentages of the downregulated exons (Fig. S4 for the motifs of highest enrichment). Such a high enrichment of a binding motif in the up-regulated exons was not detected.

Taken together these results show IQGAP1's involvement in AS regulation. Its RNA-independent interaction with hnRNPM stands out as a distinct one, as the two proteins are predicted to regulate common AS events related to cell cycle and cell division.

Nuclear IQGAP1 interacts with hnRNPM to control its regulatory role in splicing

The interaction of nuclear IQGAP1 with hnRNPM was confirmed *in situ* using the proximity ligation assay (PLA) (Fig. 4A), with the β-actin-IQGAP1 interaction (37) serving as a positive control (Fig. S5A). Quantification of the cytoplasmic and nuclear PLA signal per cell demonstrated that the interaction between hnRNPM and IQGAP1 is mainly nuclear (Fig. 4B). Some cytoplasmic interaction sites were detected, but they were minor compared to the nuclear ones (Fig. 4A-B). In agreement with these results, immunoprecipitation from cytoplasmic extracts using anti-IQGAP1 antibodies did not reveal an interaction with the minor amounts of cytoplasmic hnRNPM (Fig. S5B). Thus, if the cytoplasmic proteins interact, these complexes are less abundant compared to the nuclear ones. The IQGAP1-hnRNPM interaction appears to be DNA-independent as it is still detected after immunoprecipitation in the presence of DNase (Fig. S5C).

To assess the involvement of IQGAP1 in hnRNPM-regulated splicing, we transfected *IQGAP1*^{KO} and parental STAD cell lines with the hnRNPM-responsive DUP51M1 and the hnRNPM-non-responsive DUP51-ΔM plasmids and analysed as described above. DUP51-ΔM was derived from DUP51M1 by mutating the hnRNPM binding site in exon 2. This results in increased exon 2 inclusion compared to the DUP51M1 reporter, due to loss of hnRNPM binding (28) (compare lanes 1, 2 of Fig. 4C and Fig. 4D). Though the splicing pattern of both reporters was affected upon *IQGAP1*-loss, the effect of IQGAP1^{KO} on the AS of the hnRNPM-responsive reporter, DUP51M1 (compare lanes 1, 3 of Fig. 4C and Fig. 4D) was more prominent compared to the effect on the AS of the hnRNPM non-responsive reporter, DUP51-ΔM (compare lanes 2, 4 of Fig. 4C and Fig. 4D). Thus, even though IQGAP1 participates in hnRNPM-independent AS regulation, not surprising since it interacts with a large number of splicing factors in nuclear RNPs (Fig. 2), the effect of *IQGAP1*^{KO} on hnRNPM-dependent AS is more significant. IQGAP1 deletion affects hnRNPM-dependent AS regulation to levels similar to the ones imposed by the loss of hnRNPM binding to the pre-mRNA (compare lanes 2, 3 in Fig. 4C and Fig. 4D). UV-crosslinking and subcellular fractionation experiments (Supplementary Results) revealed that IQGAP1 does not regulate the binding of hnRNPM to its RNA target (Fig. S5D) and it is not component of the Large Assembly of Spliceosome Regulators (LASR) (Fig. S5E). Thus, IQGAP1 participates in hnRNPM-dependent AS regulation.

IQGAP1 regulates hnRNPM's splicing activity by controlling its subnuclear distribution

It is known that changes in the subnuclear/subcellular distribution of splicing factors affects AS outcome (38–40). For hnRNPM, two cases of changes in its subnuclear distribution have been connected to altered splicing outcome: i. hnRNPM's response to heat-shock by relocalizing from the nucleoplasm towards the nuclear matrix (22); ii. hnRNPM's response to

224 a chemotherapeutic inhibitor (BEZ235) of the PI3K/mTOR pathway (41). To evaluate
225 whether IQGAP1 affects hnRNPM-regulated AS by interfering with hnRNPM's subnuclear
226 distribution, we used immunofluorescence and confocal microscopy. A subtle but noticeable
227 and quantifiable change in the subnuclear distribution of hnRNPM was detected upon
228 IQGAP1 depletion, with the perinuclear enriched localization in parental cells changing to a
229 diffused distribution, not only at the periphery, but also deeper within the nuclei (Figs. 5A-B,
230 S6A-B).

231 To detect whether in *IQGAP1*^{KO}, hnRNPM can be further displaced by heat- or BEZ235
232 treatment, we assayed MKN45 cells and the *IQGAP1*^{KO} derivatives for localization of
233 hnRNPM under these two treatment conditions. The localization of hnRNPM changed upon
234 heat-shock from its mostly perinuclear pattern in untreated parental cells to a more diffused
235 one, less localized at the periphery, in the heat-shocked cells (Figs. 5C upper panels, S6A-
236 D). Surprisingly, hnRNPM's localization pattern did not change upon heat-shock in
237 *IQGAP1*^{KO} cells (Figs. 5C lower panels, S6A, D), showing the necessity of IQGAP1 for
238 hnRNPM's response to heat-induced stress. Though we could clearly detect the effect of
239 BEZ235 treatment on hnRNPM's subnuclear distribution in parental, the results we got for
240 *IQGAP1*^{KO} cells were not as clear and quantifiable as those with heat-shock (Fig. S6C).
241 Therefore, we used heat-shock to further characterise the involvement of IQGAP1 in
242 hnRNPM's subnuclear distribution.

243 To probe how the localization of hnRNPM relates to AS outcome, we compared hnRNPM's
244 subnuclear localization to that of SR splicing regulators, in untreated and heat-shocked
245 parental and *IQGAP1*^{KO} cells. Upon heat-shock, colocalization between hnRNPM and SR
246 proteins was reduced in parental cells. hnRNPM and SR proteins showed also similarly
247 decreased colocalization in untreated *IQGAP1*^{KO} cells, and importantly, no further change
248 was induced upon heat-shock in these cells (Figs. 5C, S6E). Furthermore, heat-shock
249 affected the localization of the signal generated by the anti-SR antibody changed upon heat-
250 shock, showing that at least some of the detected SR factors respond to heat-induced stress

by altering subnuclear distribution, however, these changes happen only in the presence of IQGAP1 (Fig. 5C). Segmentation of the nuclei in 4 sub-regions revealed that the reduction in colocalization was not constrained in a particular region of the nucleus, but it was rather similar in all subnuclear segments (Figs. 5D, S6F).

To test whether the involvement of IQGAP1 in the heat-induced subnuclear re-localization of AS regulators is linked to their splicing activity, we assayed the AS pattern of the hnRNPM-responsive DUP50M1 minigene reporter upon heat-shock in *IQGAP1*^{KO} and parental cells. In agreement with the above observations and previous reports on the impact of heat-shock on the splicing machinery (42–44), heat-shock resulted in change of the AS pattern of the reporter (Fig. 5E, lanes 1-2). However, such an effect was not apparent in *IQGAP1*^{KO} cells (Fig. 5E, lanes 3-4). No effect of heat-shock was observed on the AS pattern of the hnRNPM non-responsive reporter (DUP50-ΔM) under these conditions (Fig. 5F, lanes 1-4) independently of the presence of IQGAP1. Thus, IQGAP1 is required for the hnRNPM's response to heat-shock, and mediates the response of the splicing machinery to heat-induced stress through its effect on hnRNPM.

IQGAP1 regulates the exchange of hnRNPM between the nuclear matrix and the splicing machinery

To gain further insight into how IQGAP1 mediates the response of hnRNPM and the splicing machinery to heat-shock, we compared nuclear matrix preparations from parental and *IQGAP1*^{KO} cells before and after heat-shock. Elevated hnRNPM levels were detected in the nuclear matrix of the parental cells after heat-shock compared to untreated cells, whereas such change was not detected in the *IQGAP1*^{KO} cells (Fig. 6A). Critically, IQGAP1 levels were also increased in nuclear matrix fractions prepared from heat-shocked cells (Fig. 6A), in agreement to the increased nuclear IQGAP1 staining detected in heat-shocked cells, compared to the untreated controls (Fig. S7A).

Using confocal microscopy and immunofluorescence staining, we compared the localization of hnRNPM with PSF (SFPQ) which is enriched in the nuclear matrix, where it interacts and colocalizes with hnRNPM, whereas PSF also interacts with splicing regulators in the soluble nucleoplasm (e.g. PTB) (45,46). Colocalization between hnRNPM and PSF was partial in untreated parental cells, and was significantly increased upon heat-shock (Figs. 6B, S7B-C) confirming that hnRNPM moves closer to PSF, possibly in the nuclear matrix. In untreated *IQGAP1*^{KO} cells, there was increased colocalization between hnRNPM and PSF compared to parental cells, and no significant further change was observed upon heat-shock (Figs. 6B, S7B-C). Quantification after segmentation of the signal in subnuclear regions supported these observations and further showed that the distribution pattern of the colocalized signal in the *IQGAP1*^{KO} cells (both untreated and heat-shocked) resembled more that of the heat-shocked parental cells especially at the outer nucleoplasm (Nucleoplasm 2) and the nuclear periphery (Figs. 6C, S7C). Therefore, IQGAP1 is critical for the changes in hnRNPM's subnuclear distribution during heat-shock in STAD cells.

IQGAP1 drives the response of hnRNPM to heat-shock and the dependence of this response to active sumoylation

HnRNPM is sumoylated by SUMO2 in untreated HeLa cells (47) and as such it is a component of early spliceosomal complexes (48). In response to heat-shock hnRNPM-SUMO2 conjugation is increased (24,26,49,50). Furthermore, upon heat-shock the association of hnRNPM with components of the active spliceosome is diminished (12), it appears enriched in nuclear matrix preparations and its presence in the nucleoplasm is reduced (22). Therefore, sumoylation of hnRNPM has an involvement in its localization within the nucleus, in relation to spliceosomal and nuclear matrix components. To explore whether IQGAP1 regulates hnRNPM's sumoylation status, we immunoprecipitated hnRNPM from *IQGAP1*^{KO} and parental untreated and heat-shocked cells. Analysis of the pulled-down

material by immunoblot with anti-hnRNPM antibodies showed that in addition to the bands of hnRNPM (~70kDa), we could detect proteins of higher molecular weight (differing ~20 and up to 100 kDa from hnRNPM, a shift consistent with hnRNPM being modified by SUMO at a single or more lysine residues) that were enriched in the *IQGAP1*^{KO} (untreated and heat-shocked) and in the parental heat-shocked cells, compared to the untreated cells (Fig. S8A). We confirmed that these higher molecular weight species corresponded to SUMO2/3-conjugates by immunoblotting with anti-SUMO2/3 antibodies (Fig. 7A). Increased amounts and number of sumoylated hnRNPM species were pulled down by the anti-hnRNPM Ab from nuclear extracts derived from heat-shocked cells compared to the untreated controls. Similarly, increased amount and number of SUMO conjugates were pulled-down from extracts derived from *IQGAP1*^{KO} cells (both untreated and heat-shocked), compared to untreated parental cells (Fig. 7A). Immunoblotting with anti-SUMO1 antibodies did not detect hnRNPM-SUMO1 conjugates in the immunoprecipitated proteins (data not shown). To further support this finding, we detected sumoylated hnRNPM and compared its levels in parental and *IQGAP1*^{KO} cells by the PLA assay using anti-hnRNPM and anti-SUMO2/3 antibodies (51) (Fig. 7B). The levels of sumoylated hnRNPM were significantly increased in untreated *IQGAP1*^{KO} cells compared to the parental cells (Fig. 7B). Smaller differences were detected in sumoylated-hnRNPM levels between the heat-shocked cells (both parental and *IQGAP1*^{KO}) and untreated *IQGAP1*^{KO} cells.

To assay the dependence of the subnuclear distribution of hnRNPM on sumoylation, we used the Sumoylation inhibitor III 2-D08, which blocks specifically the transfer of SUMO from the Ubc9 thioester to SUMO substrates (52). After verifying that 2-D08 blocked general SUMO2/3 conjugation but also SUMO2/3-hnRNPM conjugation (Fig. S8B-C), we tested whether heat-shock induced changes on hnRNPM localization depend on active sumoylation, using immunofluorescence and confocal microscopy (Figs. 7C, S8D). Heat-stress induced the expected increase of hnRNPM towards the center of the cells in the absence of 2-D08 (Fig. 7C), whereas in its presence, hnRNPM's subnuclear distribution resembled the one in

330 untreated cells (Figs. 7C, DMSO no HS and S8D). This was not the case in *IQGAP1*^{KO} cells,
331 where hnRNPM's distribution and sumoylation levels are similar to the heat-shocked
332 parental cells; the distribution of hnRNPM in these cells, was hardly altered upon inhibition of
333 SUMO conjugation, supporting the finding that hnRNPM's subnuclear distribution depends
334 firstly on the presence of IQGAP1 (Figs. 7D, S8D).

335 Taken together, these results show that IQGAP1 regulates hnRNPM's AS-activity,
336 sumoylation status and proper localization in the nucleus.

337

338 **IQGAP1 and hnRNPM co-regulate the function of APC/C through AS of the ANAPC10**
339 **pre-mRNA and promote gastric cancer cell growth *in vitro* and *in vivo***

340 Given the role of IQGAP1 as a regulator of hnRNPM's splicing activity and its significance for
341 the survival of STAD patients (Fig. S9A) we assessed whether AS events regulated by both
342 IQGAP1 and hnRNPM contribute to STAD progression. From the AS events detected in our
343 genome-wide analyses (Fig. 3) *ANAPC10* pre-mRNA was singled out for further study as it
344 had the highest change in |ΔPsi|/Psi combination (Fig. 8A, Table S2a). *ANAPC10* pre-mRNA
345 is an hnRNPM-eCLIP target (53) with the major hnRNPM binding site and the predicted
346 hnRNPM consensus binding motif located downstream of exon 4 (Fig. S9B). Downregulation
347 of this event corresponds to better survival of STAD patients (Fig. S9C). ANAPC10 is critical
348 for cell cycle and cell division, as the substrate recognition component of the APC/C, a cell
349 cycle-regulated E3-ubiquitin ligase controlling progression through mitosis and the G1 phase
350 of the cell cycle. ANAPC10 interacts with the co-factors CDC20 and/or CDH1 to recognize
351 targets to be ubiquitinated and subsequently degraded by the proteasome (54–56).

352 In *IQGAP1*^{KO} cells, decreased levels of *ANAPC10* exon 4 inclusion were detected (Fig. 8B).
353 Using siRNAs against hnRNPM in *IQGAP1*^{KO} cells to simultaneously reduce IQGAP1 and
354 hnRNPM levels, we noticed further decrease of *ANAPC10* exon 4 inclusion (Fig. 8B). Exon 4
355 skipping results in production of an isoform lacking amino-acid residues important for

interaction with the D-box of the APC/C targets (57,58). Using LC-MS/MS analyses of the proteomes of the parental and the *IQGAP1*^{KO} cell lines, we compared the levels of known targets of the APC/C complex (Fig. 8C) and detected increased abundance of anaphase-specific targets of the APC/C-CDH1 (55), namely RRM2, TPX2, ANLN, and TK1, but not of other APC/C known targets (Fig. 8C). Immunoblotting using specific antibodies verified these results (Fig. S9D). The same was true for CDH1/FZR, an APC/C co-factor, which is also a target of the complex, as is ANLN (Fig. S9E). Interestingly, survival plots for RRM2 and TK1 connect increased expression of the respective mRNAs with better prognosis for survival for STAD patients (Fig. S9F-G).

To assess the effect of such a phenotype in gastric cancer cell growth, we used a CRISPR-Cas9 approach to generate *hnRNPM*^{KO} and double KO cells (see Supplementary Materials and Fig. S10A). Since the RNA-seq analyses revealed that the IQGAP1-regulated AS events are cell cycle-related, we first performed cell cycle analyses using propidium iodide combined with flow cytometry. Unsynchronized *IQGAP1*^{KO} cells had a small but significant increase in cell populations at the S and G2/M phases with subsequent reduction of cells at the G1 phase (Fig. 8D). *hnRNPM*^{KO} cells showed a similar phenotype, whereas downregulation of both proteins (in *hnRNPM*^{KO}-*IQGAP1*^{KO} cells) enhanced this effect (Fig. 8D). These differences were more pronounced after cell cycle synchronization (Fig. S10B).

To further delineate this phenotype and given the role of APC/C in the progression of mitosis and cell division (55,57,59,60) we assayed the impact of the downregulation of both *IQGAP1* and *hnRNPM* on cell division. Using DAPI staining and anti-β-tubulin cytoskeleton immunostaining we detected a significant number of double *KO* cells being multinucleated (Figs. 8E, S10C). Similar phenotype was detected when siRNAs were used to downregulate hnRNPM levels (data not shown). hnRNPM and IQGAP1 together support proliferation but do not control migration of gastric cancer cells (Supplementary Results, Fig. S10D-E).

To examine the *in vivo* effect of the absence of IQGAP1 and hnRNPM on tumour development and progression, we injected the MKN45-derived cell lines (MKN45, MKN45-*IQGAP1*^{KO}, MKN45-*hnRNPM*^{KO} and MKN45-*hnRNPM*^{KO}-*IQGAP1*^{KO}) subcutaneously into the flanks of NOD/SCID mice. Tumor dimensions were measured throughout the experiment. Cells with reduced levels of both IQGAP1 and hnRNPM resulted in significantly reduced tumour growth compared to the parental and the single KO cells (Fig. 8F). Immunohistochemical analysis of the tumours confirmed reduced levels of hnRNPM and/or IQGAP1 in the cell lines-derived xenografts. Furthermore, Ki-67 staining was significantly reduced in the single and double KO tumours compared to the parental cell line-derived ones, showing the involvement of the two proteins in the *in vivo* proliferation of gastric cancer cells (Fig. S10F).

Collectively, IQGAP1 and hnRNPM co-operatively generate at least an alternatively spliced isoform of ANAPC10. This, in turn, tags cell cycle-promoting proteins for degradation and contributes to the accelerated proliferation phenotype of tumour cells.

DISCUSSION

Splicing regulatory networks are subject to signals modulating alternative exon choice. In response to heat-induced stress, shutdown, mainly of post-transcriptional pre-mRNA splicing, has been reported (44,61). However, it is still unknown how heat-induced signals reach their targets and affect the AS regulatory components of the spliceosome. Here, we provide conclusive evidence for the role of a scaffold protein, IQGAP1, in mediating the response of AS regulators to heat-induced stress.

We show that nuclear IQGAP1 interacts with a large number of splicing factors mostly in an RNA-dependent manner. Focusing on its RNA-independent interaction with hnRNPM, we show that only in the presence of IQGAP1, hnRNPM responds to heat-induced stress, by moving away from spliceosome components towards the less-well-defined nuclear matrix.

This response of hnRNPM to heat-shock is dependent on active sumoylation. Tools like the Protease-Reliant Identification of SUMO Modification (PRISM) or the Lysine deficient (K0) techniques ((26,27,50)) that allow detection of sumo-conjugated peptides have revealed at least 10 peptides of hnRNPM that are SUMO2 conjugated not only in untreated cells but also after heat shock (27). Additional, meticulous experiments will be needed to reveal the sumoylation site(s) of hnRNPM that play key roles to its functionality in AS and its interaction with IQGAP1. However, given that not only hnRNPM (work presented herein, and (47,49,62,63)), but also IQGAP1, as it has been reported previously and also verified by us ((64) and data not shown), are sumoylated, the dependence of hnRNPM's response to heat-shock on specific sumoylation events needs to be carefully and cautiously validated. Because hnRNPM is critical for the response of the spliceosome to heat-shock (22,42), the effect of IQGAP1 on hnRNPM's participation in AS events can be deterministic for the response of the splicing machinery to heat-induced stress.

Furthermore, the absence of IQGAP1 alone triggers similar effect on hnRNPM as heat-shock. In *IQGAP1*^{KO} cells, hnRNPM is already in a "splicing-inactive" sumoylation state, close to nuclear matrix components as it is in heat-shocked cells. In this state, hnRNPM's regulatory role in splicing changes even though it can still bind its pre-mRNA target. Therefore, IQGAP1 is necessary for efficient splicing activity of hnRNPM by controlling its proper localization. The fact that IQGAP1 is a scaffold protein with well-known roles in the cytoplasm as signal integrator suggests that the involvement of IQGAP1 in the response of AS to stress signals may be a generalized phenomenon.

The nuclear localization of IQGAP1 appears to be cell-cycle dependent (13,65). hnRNPM is required for progression of the cell cycle G1 phase (66). In the absence of IQGAP1, pre-mRNAs involved in cell cycle regulation undergo differential AS, half of which are co-regulated by hnRNPM. The AS event involving *ANAPC10*, results in inactive APC/C and stabilization of at least a group of APC/C-CDH1 targets. Given the central role played by the

controlled degradation of these proteins for cell cycle progression (55,67), we posit that regulation of the relevant AS event constitutes one newly reported way to control cell cycle.

Currently, the literature on signal regulated AS, cell cycle control and tumour growth is rather fragmentary. Our results identify at least one missing link between extra-nuclear signals and AS in gastric cancer cells. Looking at the bigger picture, it will be interesting to test this regulation in the case of normal cells and assess the possibility that the interaction of IQGAP1 with splicing regulators e.g. hnRNPM could be targeted for development of very specific therapeutic approaches.

ACKNOWLEDGEMENTS

We thank N. Boni-Kazantzidou and G.-R. Manikas for the generation of crucial preliminary data; P. Hantzis, M. Fousteri, V. Koliaraki (IFBR, B.S.R.C. “Al. Fleming”) and N. Balatsos (University of Thessaly, Greece) for cell lines and reagents; D. Black and A. Damianov (UCLA, USA) for plasmids and technical advice on minigene reporter splicing assays; A. Guialis (N.H.R.F., Athens, Greece) for antibodies and reagents; Per Haberkant and the EMBL Proteomics Core Facility for LC-MS/MS analyses and advice; Sofia Grammenoudi and the Flow cytometry facility of B.S.R.C. “Al. Fleming” for help with cell cycle analyses and discussions; Vladimir Benes, Jonathan Landry and the EMBL Genecore for RNA-seq analyses and discussions; Martina Samiotaki, George Stamatakis at the Proteomics Facility of B.S.R.C. “Al. Fleming” for LC-MS/MS analyses and discussions; the personnel of the Imaging facility of B.S.R.C. “Al. Fleming” for help with image acquisition. We also thank George Panayotou and Efthimios Skoulakis (B.S.R.C. “Al. Fleming”) for critical reading of the manuscript; Juan Valcarcel for help with the analysis of the RNA-seq data; Skarlatos G. Dedos (National and Kapodistrian University of Athens, Greece) for reagents, plasmids, discussions and critical reading of the manuscript.

FUNDING

InfrafrontierGR/Phenotypos Infrastructure, co-funded by Greece and the European Union (European Regional Development Fund) [NSRF 2014-2020, MIS 5002135]; Hellenic Foundation for Research & Innovation (HFRI) and the General Secretariat for Research and Technology (GSRT) [grant agreement 846 to Z.E.]; M.R. was supported by the European Research Council [ERC AdvG 670146]; European Commission Grant FP7-PEOPLE-2010-IEF [274837] to P.K; Stavros Niarchos Foundation (SNF) donation to BSRC “Al. Fleming”.

Author contributions

These authors contributed equally: Andrada Birladeanu, Malgorzata Rogalska, Myrto Potiri. A.B. performed most of the immunofluorescence, subcellular fractionation, immunostaining and *in vitro* splicing experiments. M.R. performed all the statistical and bioinformatics analyses. M.P. performed the cellular assays (cell cycle, wound healing, colony formation, MTT assays) and CRISPR-Cas9 editing experiments. Z.E. performed RT-PCR analyses and supervised A.B in *in vitro* splicing assays and M.P in cell cycle analyses. V.P. performed immunofluorescence analyses, western blotting analyses, advised A.B. on image acquisition and analyses, supervised M.P. on cellular assays. M.A. and P.K. performed the xenograft experiments. D.L.K. advised M.A. and helped with the cellular assays. J.D.L. helped with the CRISPR-Cas9 editing experiments. P.K conceived, designed and supervised the study, performed the immunoprecipitation experiments and wrote the manuscript. All authors edited and commented on the manuscript.

REFERENCES

1. Pan Q, Shai O, Lee LJ, Frey BJ, Blencowe BJ. Deep surveying of alternative splicing complexity in the human transcriptome by high-throughput sequencing. Nat Genet [Internet]. 2008 Dec

[cited 2017 Mar 30];40(12):1413–5. Available from:
http://www.nature.com/ng/journal/v40/n12/abs/ng.259.html

2. Wang Z, Burge CB. Splicing regulation: From a parts list of regulatory elements to an integrated splicing code. RNA [Internet]. 2008 May 1 [cited 2015 Feb 27];14(5):802–13. Available from: http://rnajournal.cshlp.org/content/14/5/802

3. Oltean S, Bates DO. Hallmarks of alternative splicing in cancer. Oncogene. 2013 Dec 16;

4. Sveen A, Kilpinen S, Ruusulehto A, Lothe RA, Skotheim RI. Aberrant RNA splicing in cancer; expression changes and driver mutations of splicing factor genes. Oncogene. 2015 Aug 24;

5. El Marabti E, Younis I. The Cancer Spliceome: Reprograming of Alternative Splicing in Cancer. Front Mol Biosci [Internet]. 2018 Sep 7 [cited 2019 Apr 26];5. Available from: https://www.ncbi.nlm.nih.gov/pmc/articles/PMC6137424/

6. Kahles A, Lehmann K-V, Toussaint NC, Hüser M, Stark SG, Sachsenberg T, et al. Comprehensive Analysis of Alternative Splicing Across Tumors from 8,705 Patients. Cancer Cell [Internet]. 2018 Aug 13 [cited 2019 Aug 13];34(2):211-224.e6. Available from: http://www.sciencedirect.com/science/article/pii/S1535610818303064

7. Cherry S, Lynch KW. Alternative splicing and cancer: insights, opportunities, and challenges from an expanding view of the transcriptome. Genes Dev [Internet]. 2020 Aug 1 [cited 2020 Oct 9];34(15–16):1005–16. Available from: http://genesdev.cshlp.org/content/34/15-16/1005

8. Langeberg LK, Scott JD. Signalling scaffolds and local organization of cellular behaviour. Nat Rev Mol Cell Biol [Internet]. 2015 Apr [cited 2020 Oct 9];16(4):232–44. Available from: https://www.ncbi.nlm.nih.gov/pmc/articles/PMC4722875/

9. Rosenbaum JC, Fredrickson EK, Oeser ML, Garrett-Engele CM, Locke MN, Richardson LA, et al. Disorder targets misorder in nuclear quality control degradation: a disordered ubiquitin ligase directly recognizes its misfolded substrates. Mol Cell. 2011 Jan 7;41(1):93–106.

10. Suganuma T, Mushegian A, Swanson SK, Abmayr SM, Florens L, Washburn MP, et al. The ATAC acetyltransferase complex coordinates MAP kinases to regulate JNK target genes. Cell. 2010 Sep 3;142(5):726–36.

11. Rappsilber J, Ryder U, Lamond AI, Mann M. Large-Scale Proteomic Analysis of the Human Spliceosome. Genome Res [Internet]. 2002 Aug [cited 2018 Feb 5];12(8):1231–45. Available from: https://www.ncbi.nlm.nih.gov/pmc/articles/PMC186633/

12. Llères D, Denegri M, Biggiogera M, Ajuh P, Lamond AI. Direct interaction between hnRNP-M and CDC5L/PLRG1 proteins affects alternative splice site choice. EMBO Rep. 2010 Jun;11(6):445–51.

13. Johnson M, Sharma M, Brocardo MG, Henderson BR. IQGAP1 translocates to the nucleus in early S-phase and contributes to cell cycle progression after DNA replication arrest. Int J Biochem Cell Biol. 2011 Jan;43(1):65–73.

14. Smith JM, Hedman AC, Sacks DB. IQGAPs choreograph cellular signaling from the membrane to the nucleus. Trends Cell Biol [Internet]. 2015 Mar [cited 2019 Apr 24];25(3):171–84. Available from: https://www.ncbi.nlm.nih.gov/pmc/articles/PMC4344846/

15. Sayedyahossein S, Li Z, Hedman AC, Morgan CJ, Sacks DB. IQGAP1 Binds to Yes-associated Protein (YAP) and Modulates Its Transcriptional Activity. J Biol Chem. 2016 Sep 9;291(37):19261–73.

16. Lamm N, Read MN, Nobis M, Van Ly D, Page SG, Masamsetti VP, et al. Nuclear F-actin counteracts nuclear deformation and promotes fork repair during replication stress. Nat Cell

Biol [Internet]. 2020 Dec [cited 2021 Apr 8];22(12):1460–70. Available from: https://www.nature.com/articles/s41556-020-00605-6

17. White CD, Brown MD, Sacks DB. IQGAPs in cancer: A family of scaffold proteins underlying tumorigenesis. FEBS Lett [Internet]. 2009 Jun 18 [cited 2013 Jul 3];583(12):1817–24. Available from: http://www.sciencedirect.com/science/article/pii/S0014579309003731

18. Osman MA, Sarkar FH, Rodriguez-Boulan E. A molecular rheostat at the interface of cancer and diabetes. Biochim Biophys Acta. 2013 Aug;1836(1):166–76.

19. Hu W, Wang Z, Zhang S, Lu X, Wu J, Yu K, et al. IQGAP1 promotes pancreatic cancer progression and epithelial-mesenchymal transition (EMT) through Wnt/β-catenin signaling. Sci Rep. 2019 May 17;9(1):7539.

20. Liu J, Ni X, Li Y, Chen M, Chen W, Wu Y, et al. Downregulation of IQGAP1 inhibits epithelial-mesenchymal transition via the HIF1α/VEGF-A signaling pathway in gastric cancer. J Cell Biochem. 2019 Sep;120(9):15790–9.

21. Li S, Wang Q, Chakladar A, Bronson RT, Bernards A. Gastric Hyperplasia in Mice Lacking the Putative Cdc42 Effector IQGAP1. Mol Cell Biol [Internet]. 2000 Jan 15 [cited 2013 Oct 1];20(2):697–701. Available from: http://mcb.asm.org/content/20/2/697

22. Gattoni R, Mahé D, Mähl P, Fischer N, Mattei MG, Stévenin J, et al. The human hnRNP-M proteins: structure and relation with early heat shock-induced splicing arrest and chromosome mapping. Nucleic Acids Res [Internet]. 1996 Jul 1 [cited 2018 Dec 9];24(13):2535–42. Available from: https://www.ncbi.nlm.nih.gov/pmc/articles/PMC145970/

23. Kafasla P, Patrinou-Georgoula M, Lewis JD, Guialis A. Association of the 72/74-kDa proteins, members of the heterogeneous nuclear ribonucleoprotein M group, with the pre-mRNA at early stages of spliceosome assembly. Biochem J. 2002 May 1;363(Pt 3):793–9.

24. Liebelt F, Sebastian RM, Moore CL, Mulder MPC, Ovaa H, Shoulders MD, et al. SUMOylation and the HSF1-Regulated Chaperone Network Converge to Promote Proteostasis in Response to Heat Shock. Cell Rep [Internet]. 2019 Jan 2 [cited 2020 Apr 15];26(1):236-249.e4. Available from: http://www.sciencedirect.com/science/article/pii/S2211124718319570

25. Tammsalu T, Matic I, Jaffray EG, Ibrahim AFM, Tatham MH, Hay RT. Proteome-wide identification of SUMO modification sites by mass spectrometry. Nat Protoc [Internet]. 2015 Sep [cited 2017 Mar 24];10(9):1374–88. Available from: http://www.nature.com.gate2.inist.fr/nprot/journal/v10/n9/full/nprot.2015.095.html

26. Hendriks IA, D'Souza RCJ, Yang B, Verlaan-de Vries M, Mann M, Vertegaal ACO. Uncovering global SUMOylation signaling networks in a site-specific manner. Nat Struct Mol Biol [Internet]. 2014 Oct [cited 2021 Jun 23];21(10):927–36. Available from: https://www.nature.com/articles/nsmb.2890

27. Hendriks IA, D'Souza RC, Chang J-G, Mann M, Vertegaal ACO. System-wide identification of wild-type SUMO-2 conjugation sites. Nat Commun [Internet]. 2015 Jun 15 [cited 2021 Jun 23];6(1):7289. Available from: https://www.nature.com/articles/ncomms8289

28. Damianov A, Ying Y, Lin C-H, Lee J-A, Tran D, Vashisht AA, et al. Rbfox Proteins Regulate Splicing as Part of a Large Multiprotein Complex LASR. Cell [Internet]. 2016 Apr 21 [cited 2018 Sep 28];165(3):606–19. Available from: https://www.cell.com/cell/abstract/S0092-8674(16)30338-5

29. Irimia M, Weatheritt RJ, Ellis JD, Parikshak NN, Gonatopoulos-Pournatzis T, Babor M, et al. A Highly Conserved Program of Neuronal Microexons Is Misregulated in Autistic Brains. Cell [Internet]. 2014 Dec 18 [cited 2020 Feb 27];159(7):1511–23. Available from: https://www.cell.com/cell/abstract/S0092-8674(14)01512-8

30. Gohr A, Irimia M. Matt: Unix tools for alternative splicing analysis. Bioinformatics. 2019;35(1):130–2.

31. Choi YD, Dreyfuss G. Isolation of the heterogeneous nuclear RNA-ribonucleoprotein complex (hnRNP): a unique supramolecular assembly. Proc Natl Acad Sci U S A. 1984 Dec;81(23):7471–5.

32. Kafasla P, Patrinou-Georgoula M, Guialis A. The 72/74-kDa polypeptides of the 70-110 S large heterogeneous nuclear ribonucleoprotein complex (LH-nRNP) represent a discrete subset of the hnRNP M protein family. Biochem J. 2000 Sep 1;350 Pt 2:495–503.

33. Cvitkovic I, Jurica MS. Spliceosome database: a tool for tracking components of the spliceosome. Nucleic Acids Res. 2013 Jan;41(Database issue):D132-141.

34. Ho Y-D, Joyal JL, Li Z, Sacks DB. IQGAP1 Integrates Ca2+/Calmodulin and Cdc42 Signaling. J Biol Chem [Internet]. 1999 Jan 1 [cited 2013 Oct 20];274(1):464–70. Available from: http://www.jbc.org/content/274/1/464

35. Sharma S, Findlay GM, Bandukwala HS, Oberdoerffer S, Baust B, Li Z, et al. Dephosphorylation of the nuclear factor of activated T cells (NFAT) transcription factor is regulated by an RNA-protein scaffold complex. Proc Natl Acad Sci U S A [Internet]. 2011 Jul 12 [cited 2014 Apr 24];108(28):11381–6. Available from: http://www.ncbi.nlm.nih.gov/pmc/articles/PMC3136327/

36. Popp MW-L, Maquat LE. Organizing principles of mammalian nonsense-mediated mRNA decay. Annu Rev Genet. 2013;47:139–65.

37. Johnson MA, Sharma M, Mok MTS, Henderson BR. Stimulation of in vivo nuclear transport dynamics of actin and its co-factors IQGAP1 and Rac1 in response to DNA replication stress. Biochim Biophys Acta BBA - Mol Cell Res [Internet]. 2013 Oct 1 [cited 2017 Jun

13];1833(10):2334–47. Available from:
http://www.sciencedirect.com/science/article/pii/S0167488913002255

38. Zhong X-Y, Ding J-H, Adams JA, Ghosh G, Fu X-D. Regulation of SR protein phosphorylation and alternative splicing by modulating kinetic interactions of SRPK1 with molecular chaperones. Genes Dev [Internet]. 2009 Feb 15 [cited 2020 Oct 14];23(4):482–95. Available from: https://www.ncbi.nlm.nih.gov/pmc/articles/PMC2648651/

39. van der Houven van Oordt W, Diaz-Meco MT, Lozano J, Krainer AR, Moscat J, Cáceres JF. The Mkk3/6-p38–Signaling Cascade Alters the Subcellular Distribution of Hnrnp A1 and Modulates Alternative Splicing Regulation. J Cell Biol [Internet]. 2000 Apr 17 [cited 2020 Oct 14];149(2):307–16. Available from: https://www.ncbi.nlm.nih.gov/pmc/articles/PMC2175157/

40. Heyd F, Lynch KW. Degrade, move, regroup: signaling control of splicing proteins. Trends Biochem Sci. 2011 Aug;36(8):397–404.

41. Passacantilli I, Frisone P, De Paola E, Fidaleo M, Paronetto MP. hnRNPM guides an alternative splicing program in response to inhibition of the PI3K/AKT/mTOR pathway in Ewing sarcoma cells. Nucleic Acids Res [Internet]. 2017 Dec 1 [cited 2018 Jan 22];45(21):12270–84. Available from: https://www.ncbi.nlm.nih.gov/pmc/articles/PMC5716164/

42. Mähl P, Lutz Y, Puvion E, Fuchs JP. Rapid effect of heat shock on two heterogeneous nuclear ribonucleoprotein-associated antigens in HeLa cells. J Cell Biol. 1989 Nov;109(5):1921–35.

43. Denegri M, Chiodi I, Corioni M, Cobianchi F, Riva S, Biamonti G. Stress-induced Nuclear Bodies Are Sites of Accumulation of Pre-mRNA Processing Factors. Mol Biol Cell [Internet]. 2001 Nov 1 [cited 2019 Aug 6];12(11):3502–14. Available from: https://www.molbiolcell.org/doi/10.1091/mbc.12.11.3502

44. Shalgi R, Hurt JA, Lindquist S, Burge CB. Widespread Inhibition of Posttranscriptional Splicing Shapes the Cellular Transcriptome following Heat Shock. Cell Rep [Internet]. 2014 Jun 12 [cited 2020 Feb 10];7(5):1362–70. Available from: http://www.sciencedirect.com/science/article/pii/S2211124714003465

45. Meissner M, Dechat T, Gerner C, Grimm R, Foisner R, Sauermann G. Differential nuclear localization and nuclear matrix association of the splicing factors PSF and PTB. J Cell Biochem. 2000 Jan;76(4):559–66.

46. Marko M, Leichter M, Patrinou-Georgoula M, Guialis A. hnRNP M interacts with PSF and p54(nrb) and co-localizes within defined nuclear structures. Exp Cell Res. 2010 Feb 1;316(3):390–400.

47. Vertegaal ACO, Ogg SC, Jaffray E, Rodriguez MS, Hay RT, Andersen JS, et al. A Proteomic Study of SUMO-2 Target Proteins*. J Biol Chem [Internet]. 2004 Aug 6 [cited 2021 May 13];279(32):33791–8. Available from: https://www.sciencedirect.com/science/article/pii/S0021925820774454

48. Pozzi B, Bragado L, Will CL, Mammi P, Risso G, Urlaub H, et al. SUMO conjugation to spliceosomal proteins is required for efficient pre-mRNA splicing. Nucleic Acids Res. 2017 Jun 20;45(11):6729–45.

49. Hendriks IA, Vertegaal ACO. Label-Free Identification and Quantification of SUMO Target Proteins. Methods Mol Biol Clifton NJ. 2016;1475:171–93.

50. Hendriks IA, Lyon D, Young C, Jensen LJ, Vertegaal ACO, Nielsen ML. Site-specific mapping of the human SUMO proteome reveals co-modification with phosphorylation. Nat Struct Mol Biol [Internet]. 2017 Mar [cited 2021 Jun 23];24(3):325–36. Available from: https://www.nature.com/articles/nsmb.3366

51. Matic I, Schimmel J, Hendriks IA, van Santen MA, van de Rijke F, van Dam H, et al. Site-Specific Identification of SUMO-2 Targets in Cells Reveals an Inverted SUMOylation Motif and a Hydrophobic Cluster SUMOylation Motif. Mol Cell [Internet]. 2010 Aug 27 [cited 2021 Jan 27];39(4):641–52. Available from: http://www.sciencedirect.com/science/article/pii/S1097276510005733

52. Kim YS, Keyser SGL, Schneekloth JS. Synthesis of 2′,3′,4′-trihydroxyflavone (2-D08), an inhibitor of protein sumoylation. Bioorg Med Chem Lett [Internet]. 2014 Feb 15 [cited 2021 May 27];24(4):1094–7. Available from: https://www.sciencedirect.com/science/article/pii/S0960894X14000298

53. Van Nostrand EL, Pratt GA, Shishkin AA, Gelboin-Burkhart C, Fang MY, Sundararaman B, et al. Robust transcriptome-wide discovery of RNA-binding protein binding sites with enhanced CLIP (eCLIP). Nat Methods. 2016 Jun;13(6):508–14.

54. da Fonseca PCA, Kong EH, Zhang Z, Schreiber A, Williams MA, Morris EP, et al. Structures of APC/C(Cdh1) with substrates identify Cdh1 and Apc10 as the D-box co-receptor. Nature. 2011 Feb 10;470(7333):274–8.

55. Zhou Z, He M, Shah AA, Wan Y. Insights into APC/C: from cellular function to diseases and therapeutics. Cell Div. 2016;11:9.

56. Yamano H. APC/C: current understanding and future perspectives. F1000Research. 2019;8.

57. Engström Y, Eriksson S, Jildevik I, Skog S, Thelander L, Tribukait B. Cell cycle-dependent expression of mammalian ribonucleotide reductase. Differential regulation of the two subunits. J Biol Chem [Internet]. 1985 Aug 5 [cited 2020 Feb 14];260(16):9114–6. Available from: http://www.jbc.org/content/260/16/9114

58. Alfieri C, Zhang S, Barford D. Visualizing the complex functions and mechanisms of the anaphase promoting complex/cyclosome (APC/C). Open Biol. 2017;7(11).

59. Sherley JL, Kelly TJ. Regulation of human thymidine kinase during the cell cycle. J Biol Chem. 1988 Jun 15;263(17):8350–8.

60. Neumayer G, Belzil C, Gruss OJ, Nguyen MD. TPX2: of spindle assembly, DNA damage response, and cancer. Cell Mol Life Sci CMLS. 2014 Aug;71(16):3027–47.

61. Biamonti G, Caceres JF. Cellular stress and RNA splicing. Trends Biochem Sci [Internet]. 2009 Mar 1 [cited 2019 Aug 6];34(3):146–53. Available from: http://www.sciencedirect.com/science/article/pii/S0968000409000061

62. Vassileva MT, Matunis MJ. SUMO Modification of Heterogeneous Nuclear Ribonucleoproteins. Mol Cell Biol [Internet]. 2004 May 1 [cited 2019 Apr 22];24(9):3623–32. Available from: https://mcb.asm.org/content/24/9/3623

63. Hendriks IA, Vertegaal ACO. A comprehensive compilation of SUMO proteomics. Nat Rev Mol Cell Biol [Internet]. 2016 Sep [cited 2021 Jun 23];17(9):581–95. Available from: https://www.nature.com/articles/nrm.2016.81

64. Liang Z, Yang Y, He Y, Yang P, Wang X, He G, et al. SUMOylation of IQGAP1 promotes the development of colorectal cancer. Cancer Lett [Internet]. 2017 Dec 28 [cited 2021 Mar 31];411:90–9. Available from: https://www.sciencedirect.com/science/article/pii/S0304383517306079

65. Lian AT, Hains PG, Sarcevic B, Robinson PJ, Chircop M. IQGAP1 is associated with nuclear envelope reformation and completion of abscission. Cell Cycle [Internet]. 2015 Apr 30 [cited 2017 May 24];14(13):2058–74. Available from: http://www.ncbi.nlm.nih.gov/pmc/articles/PMC4613854/

66. Santos A, Wernersson R, Jensen LJ. Cyclebase 3.0: a multi-organism database on cell-cycle regulation and phenotypes. Nucleic Acids Res [Internet]. 2015 Jan 28 [cited 2020 Mar 9];43(D1):D1140–4. Available from: https://academic.oup.com/nar/article/43/D1/D1140/2437426

67. Penas C, Ramachandran V, Ayad NG. The APC/C Ubiquitin Ligase: From Cell Biology to Tumorigenesis. Front Oncol. 2011;1:60.

68. McQuin C, Goodman A, Chernyshev V, Kamentsky L, Cimini BA, Karhohs KW, et al. CellProfiler 3.0: Next-generation image processing for biology. PLOS Biol [Internet]. 2018 Jul 3 [cited 2020 Feb 25];16(7):e2005970. Available from: https://journals.plos.org/plosbiology/article?id=10.1371/journal.pbio.2005970

69. Saraiva-Agostinho N, Barbosa-Morais NL. psichomics: graphical application for alternative splicing quantification and analysis. Nucleic Acids Res. 2019 25;47(2):e7.

70. Huelga SC, Vu AQ, Arnold JD, Liang TY, Liu PP, Yan BY, et al. Integrative Genome-wide Analysis Reveals Cooperative Regulation of Alternative Splicing by hnRNP Proteins. Cell Rep [Internet]. 2012 Feb 23 [cited 2014 Apr 29];1(2):167–78. Available from: http://www.cell.com/article/S2211124712000435/abstract

71. Rando OJ, Zhao K, Crabtree GR. Searching for a function for nuclear actin. Trends Cell Biol [Internet]. 2000 Mar 1 [cited 2020 Feb 25];10(3):92–7. Available from: https://www.cell.com/trends/cell-biology/abstract/S0962-8924(99)01713-4

FIGURE LEGENDS

Fig. 1: IQGAP1 expression levels are significantly increased in gastric cancer cells. A Representative epifluorescence images of normal and adenocarcinoma gastric tissues on a

commercial tissue microarray. Tissues were immunostained with rabbit anti-IQGAP1 antibodies. DAPI was used for nuclei staining. The same settings for IQGAP1 signal acquisition were applied in all samples. **B** Quantification of IQGAP1 fluorescence signal intensity in normal and gastric tumour samples. Cell segmentation and Integrated Intensity measurements were performed with Cell Profiler (https://cellprofiler.org/) (68). At least 285 cells were analysed in each tissue sample. Statistical analysis with one-way ANOVA showed that the mean integrated intensities of the tissue samples are significantly different (P<0.05). P values presented in the graphs were calculated with multiple comparisons ANOVA between the normal and tumour samples (**P<0.01). **C** Expression box plots showing the *IQGAP1* mRNA levels in tumour samples from esophagogastric cancers (STES) or Stomach Adenocarcinoma (STAD) patients in comparison to TCGA normal data. The expression levels are indicated in $\log_2$(TPM + 1) values. The analysis was performed using the psichomics interphase (69). The TCGA data used were: Stomach adenocarcinoma 2016-01-28, 410 samples (358 patient and 21 normal); Stomach and Esophageal carcinoma 2016-01-28, 594 samples (539 patient and 55 normal). P values were calculated using two-tailed, unpaired t-tests, where ***P < 0.001. **D** Immunoblotting of crude protein extracts from different gastric cancer cell lines against IQGAP1. β-actin was used to normalize IQGAP1 levels. Quantification was performed using ImageLab software version 5.2 (Bio-Rad Laboratories). One-way ANOVA analysis revealed statistically significant difference between the MKN45 and NUGC4 samples. AGS: gastric adenocarcinoma; MKN45: poorly differentiated gastric adenocarcinoma, liver metastasis; KATOIII: gastric carcinoma, pleural effusion and supraclavicular and axillary lymph nodes and Douglas cul-de-sac pleural; NUGC4: poorly differentiated signet-ring cell gastric adenocarcinoma, gastric lymph node. Numbers indicate MW in kDa. See also **Supplementary Fig. S1.**

Fig. 2. Nuclear IQGAP1 is a component of RNPs involved in splicing regulation. A Representative confocal images of MKN45 and NUGC4 cells stained with an anti-IQGAP1 antibody and DAPI to visualise the nuclei. Single confocal nuclear slices are shown for each

fluorescence signal and for the merged image. Cross sections of the xz and yz axes show the presence of IQGAP1 within the cell nuclei. **B** Network of protein interactions generated from the proteins that were pulled down by anti-IQGAP1 Abs from nuclear extracts of NUGC4 cells and classified as spliceosomal components. The network was generated using the igraph R package. Colours represent classes of spliceosomal components according to SpliceosomeDB (33). Vertices are scaled according to *P* values and ordered according to known spliceosomal complexes. **C** Validation of representative IQGAP1-interacting partners presented in (**B**). Anti-IQGAP1 or control IgG pull down from nuclear extracts of NUGC4 and MKN45 cells were immunoprobed against IQGAP1, hnRNPA1, hnRNPA2/B1, hnRNPC1/C2, hnRNPL, hnRNPM and DHX9. The immunoprecipitated proteins were compared to 1/70th of the input used in the pull down. Where indicated, RNase A was added in the pull down for 30 min. Numbers indicate MW in kDa. Quantification of the IQGAP1 and hnRNPM band intensities was performed using ImageLab (BioRad) in arbitrary units. The ratio of hnRNPM/IQGAP1 intensities are presented together with the respective standard error of the mean (SEM) values. Two-tailed unpaired t-test analysis revealed statistically significant difference between NUGC4 untreated and RNaseA treated samples ($p<0.0001$). See also Supplementary **Fig. S2**.

Fig. 3. **IQGAP1 participates in alternative splicing regulation in gastric cancer cell lines. A** MKN45 and MKN45-*IQGAP1*^{KO} cells were transfected with the DUP51M1 minigene general splicing reporter (28) for 40 hrs. Upper panel: Exon 2 (grey box) splicing was assessed by RT-PCR using primers located at the flanking exons. Quantification of exon 2 inclusion was performed using ImageJ. Data shown represent the average % of exon 2 inclusion values together with the respective standard deviation (SD) values from at least 3 independent experiments. Two-tailed unpaired t-test analysis revealed statistically significant difference between MKN45 and MKN45-*IQGAP1*^{KO} cells ($p<0.0001$). Lower panel: IQGAP1 and hnRNPM levels were monitored by immunoblot. β-actin was used as a loading control. **B** MKN45 and MKN45-*IQGAP1*^{KO} cells were co-transfected with the DUP50M1 minigene

general splicing reporter (28) and pcDNA3.1 or pcDNA3.1-Myc-IQGAP1 (Ref, 4 or 5 μg) for 48 hrs. Upper panel: Exon 2 splicing was quantified as decribed in (A). Lowe panel: Endogenous and exogenous IQGAP1 expression was verified by immunoblot with anti-IQGAP1 and anti-myc antibodies. β-actin was used as a loading control. **C** Pie chart presenting the frequency of the different types of AS events (exon skipping, intron retention, alternative splice donor and alternative splice acceptor) regulated by IQGAP1 in MKN45 cells. **D** Histogram showing the results from the GO Biological process enrichment analysis of the AS events that are significantly affected by IQGAP1 deletion. **E-F** Analysis by RT-PCR and gel electrophoresis of cell cycle-related AS events in MKN45 and MKN45-*IQGAP1*^{KO} cells (all 19 events are shown in Supplementary **Tables S3, S4**). In (**E**), 6 events are presented whose inclusion was down-regulated upon *IQGAP1*^{KO} in MKN45 cells (*SDCCAG3*, *FIP1L1*, *ACOT9*, *CROCC*, *MRI1* and *ANAPC10*). In (**F**), 6 events are presented whose inclusion was up-regulated in MKN45-*IQGAP1*^{KO} compared to MKN45 (*ARHGAP27*, *TRPM4*, *RBM10*, *PSIP1*, *CENPV* and *KIF2A*). % inclusion represents the mean together with the standard deviation (SD) values of at least 3 biological replicates. Two-tailed unpaired t-test analysis revealed statistically significant difference between MKN45 and MKN45-*IQGAP1*^{KO} cells ($p<0.05$). Molecular lengths (bp) are marked on the right of each picture. When more than two PCR products are detected, in red are the products that result from the AS event of interest and were considered in the quantification of % inclusion, whereas in grey are the products that were not considered in quantification. **G** RNA map representing the distribution of hnRNPM binding motif in hnRNPM regulated exons and flanking introns, compared to control exons. Thicker segments indicate regions in which enrichment of hnRNPM motif is significantly different. The reported hnRNPM motifs (70) were identified only down-stream of the down-regulated exons. See also Supplementary **Figs. S3 and S4**.

Fig. 4. Nuclear IQGAP1 interacts with hnRNPM to control its regulatory role in splicing. **A-B** Proximity ligation assay (PLA) in MKN45 and NUGC4 cells showing the direct nuclear interaction between hnRNPM and IQGAP1. In **(A)** representative images display a central

plane from confocal z-stacks for the 2 cell lines. Negative control (secondary antibody only, MKN45 C and NUGC4 C) samples show minimal background signal. In **(B)**, quantification of the nuclear (n.MKN45 and n.NUGC4) and cytoplasmic signal (c.MKN45 and c.NUGC4) was performed per cell using the DuoLink kit-associated software. Each plot represents at least 15 cells analysed. *P* values were calculated using ANOVA multiple comparisons tests; ****$P < 0.0001$. **C-D** MKN45 and MKN45-*IQGAP1*^{KO} cells were transfected with the DUP51M1 (hnRNPM responsive) or DUP51-ΔM (hnRNPM non-responsive) minigene splicing reporters (28) for 40 hrs. Exon 2 (grey box) splicing was assessed by RT-PCR using primers located at the flanking exons. Quantification of exon 2 inclusion was performed using ImageJ. Data shown in (D) represent the average exon 2 inclusion values ± SD from at least 3 independent experiments. *P* values were calculated using unpaired, two-tailed, unequal variance Student´s t-test. See also Supplementary **Fig. S5**.

Fig. 5. IQGAP1 regulates hnRNPM's splicing activity by controlling its subnuclear distribution in cancer cells. A-B Single confocal planes of MKN45 and MKN45-*IQGAP1*^{KO} cells stained for hnRNPM, IQGAP1 and DAPI **(A)**. hnRNPM signal alone is shown in grey for better visualisation and merged images with all three coloured signals are shown on the side. Quantification in **(B)** of the intensity of the hnRNPM signal. Intensity Distribution analysis was performed as described in Materials and Methods for 40 cells per cell line. Data represent mean values ± SD. *P* values were calculated using unpaired, two-tailed t-tests; ****$P < 0.0001$, **$P < 0.01$ **C** Representative stacks from confocal images of MKN45 and MKN45-*IQGAP1*^{KO} cells untreated or after heat-shock (42^{o}C, 1 h, HS) stained for hnRNPM and SR proteins (SRp75, SRp55, SRp40, SRp30a/b and SRp20). For each condition the single and merged signals of the 2 proteins are shown on top. A single cell stained for hnRNPM and SR is shown on the bottom together with the plot profile line drawn in Image J, while the accompanying pixel grey value graphs are visible on the right of the image. **D** Quantification of Pearson's correlation coefficient values for hnRNPM and SR co-localisation, for MKN45 and MKN45-*IQGAP1*^{KO} cells before and after heat-shock stress induction. Pixel-

based co-localisation was performed for the different sub-nuclear regions (as explained in Materials and Methods) in at least 32 cells for each condition, and data represent mean values ± SD. *P* values were calculated using unpaired, two-tailed, t-tests; ****$P < 0.0001$, ***$P < 0.001$ between all conditions versus MKN untreated cells. *P* values of all other comparisons are presented in detail in Fig. S6F. **E-F** MKN45 and MKN45-*IQGAP1*^{KO} cells were transfected with the DUP50M1 (hnRNPM responsive, **(E)**) or DUP50-ΔM (hnRNPM non-responsive, **(F)**) minigene splicing reporters (28) for 40 hrs. Exon 2 (grey box) splicing was assessed by RT-PCR before (untreated, U) or after heat-shock (42^{o}C 1h, HS). Quantification of exon 2 inclusion was performed using ImageJ. Data shown represent the average exon 2 inclusion values ± SD from at least 3 independent experiments. *P* values were calculated using unpaired, two-tailed, unequal variance Student´s t-test. See also Supplementary **Fig. S6**.

Fig. 6. IQGAP1 regulates the exchange of hnRNPM between the nuclear matrix and the splicing machinery. A Immunoblot of nuclear matrix extracts from MKN45 and MKN45-*IQGAP1*^{KO} cells before (-HS) and after heat-shock (45^{o}C, 15 min, + HS) probed against hnRNPM and IQGAP1. β-actin is used as a loading control (71). Quantification of the relevant protein amounts, in arbitrary units, was performed using ImageLab software version 5.2 (Bio-Rad Laboratories). **B** Representative confocal planes of MKN45 and MKN45-*IQGAP1*^{KO} cells before (untreated) and after heat-shock stress induction for 1h at 42°C (HS), stained for hnRNPM and PSF. For each cell type and condition both the single and merged signals of the 2 proteins are shown on top. A slice from a single cell stained for hnRNPM and PSF is visible on the bottom together with the plot profile line drawn in Image J, while the accompanying pixel grey value graphs are shown on the right of the image. **C** Quantification of Pearson's correlation coefficient values of hnRNPM and PSF co-localisation for MKN45 and MKN45-*IQGAP1*^{KO} cells before (untreated) and after heat-shock stress induction for 1h at 42°C (HS). Pixel-based co-localisation was performed for the different sub-nuclear regions (as explained in Materials and Methods – see Panel B for example images) in 30

cells for each condition, and data represent mean values ± SD. *P* values were calculated using unpaired, two-tailed, t-tests; ****P < 0.0001, shown as an average between all conditions versus MKN untreated cells. *P* values of all other comparisons are presented in detail in Fig. S7C. See also Supplementary **Fig. S7**.

Fig. 7. IQGAP1 drives the response of hnRNPM to heat-shock and the dependence of this response to active sumoylation. A Anti-hnRNPM or control IgG (IgG) pull downs from nuclear extracts of MKN45 and MKN45 *IQGAP1*^{KO} cells as for (D) were analysed by an 8% SDS-PAGE. Detection of SUMO2/3 conjugated proteins was performed by immunoblot using an anti-SUMO2/3 antibody. After stripping of the antibody from the membrane, hnRNPM was also detected by immunoblot using specific antibodies (lower part) The immunoprecipitated proteins were compared to 1/70th of the input used in the pull down. Asterisks (*) indicate sumoylated hnRNPM species. **B** Proximity ligation assay (PLA) in MKN45 and MKN45-*IQGAP1*^{KO} cells, before (untreated) and after heat-shock stress induction for 1h at 42°C (HS), detecting the SUMO2/3-conjugated hnRNPM. Representative images are shown that display a central plane from confocal z-stacks. Negative control [secondary antibodies and anti-hnRNPM primary antibody only, (-) control] samples show minimal background signal. For the quantification of PLA signal the CellProfiler software was used(68) as described in Materials and Methods. Each plot represents at least 120 cells analysed. P values were calculated using ANOVA multiple comparisons tests; ****P < 0.0001. **C** Quantification of hnRNPM intensity distribution in segmented nuclei, in MKN45 cells with treated DMSO or SUMO inhibitor 2-D08. Data presented are the mean values for each condition. Statistical analysis was performed using unpaired t-tests; ****P < 0.0001, **P < 0.01. **D** Quantification of hnRNPM intensity distribution in segmented nuclei, in MKN45-*IQGAP1*^{KO} cells treated with DMSO or SUMO inhibitor 2-D08. Data presented are the mean values for each condition. Statistical analysis was performed using unpaired t-tests; ****P < 0.0001, **P < 0.01. See also **Supplementary Fig. S8**.

Fig. 8. IQGAP1 and hnRNPM co-regulate the function of APC/C through AS of the ANAPC10 pre-mRNA and promote gastric cancer cell growth *in vitro* and *in vivo*. A Scatterplot showing the distribution of the Psi values for the AS events detected by VAST-TOOLS in RNA-seq in *IQGAP1*^{KO} and control cells. In yellow are the significantly changed AS events between MKN45 and MKN45-*IQGAP1*^{KO} cells (|ΔPsi|>15, range 5), in ochre and orange are events with detected iClip binding for hnRNPM or predicted RNA-binding motif, respectively. The gene names of the events that were screened for validation are indicated. The *ANAPC10* event is shown in bold. BG: background. **B** RT-PCR (see Table S4) followed by electrophoresis was used to monitor the rate of ANAPC10 exon 4 inclusion in MKN45 and MKN45-*IQGAP1*^{KO} cells transfected with siRNAs for hnRNPM or scrambled (scr) control siRNAs. Exon 4 inclusion was quantified with ImageJ in at least 3 biological replicates. P value was calculated with unpaired t-test. **C** Volcano plot of the log2fc change in protein levels between MKN45 and MKN45-*IQGAP1*^{KO}. In red are the protein-targets of the APC/C complex that were found to be up-regulated in the KO cells. IQGAP1 and hnRNPM are also indicated. **D** Cell cycle analysis of asynchronous MKN45-derived cell lines (MKN45, MKN45-*IQGAP1*^{KO}, MKN45-*hnRNPM*^{KO} and double MKN45-*IQGAP1*^{KO}-*hnRNPM*^{KO}) using propidium iodide staining followed by FACS analysis. Quantification of the percentage of cells in each cell cycle phase was performed with FlowJo software. Data represent mean values ± SD of two independent experiments. ***$P < 0.001$, ****$P < 0.0001$. **E** Non-synchronized cells from all four cell groups were stained for β-tubulin and DAPI, to visualize the cell cytoplasm and nucleus, respectively. Quantification of the percentage of cells having 1x, 2x or >2x nuclei was performed in 20 images from each cell line, reaching a minimum number of 250 cells analysed per group. **F** MKN45, MKN45-*IQGAP1*^{KO}, *MKN45-hnRNPM*^{KO} and *MKN45-hnRNPM*^{KO}-*IQGAP1*^{KO} cells were subcutaneously injected into the flanks of NOD/SCID mice and tumours were left to develop over a period of 28 days. The tumour growth graph shows the increase of tumour volume (mm^3) over time. Tumour size was measured in anesthetised mice with a digital caliper twice per week, and at the end-point of the experiment when tumours were excised. Data presented are average values ± SD, from 11 mice per group. *P*

values were calculated using one-way ANOVA, where *P < 0.05, **P < 0.01, ****P < 0.0001. See also Supplementary **Figs. S9** and **S10**.

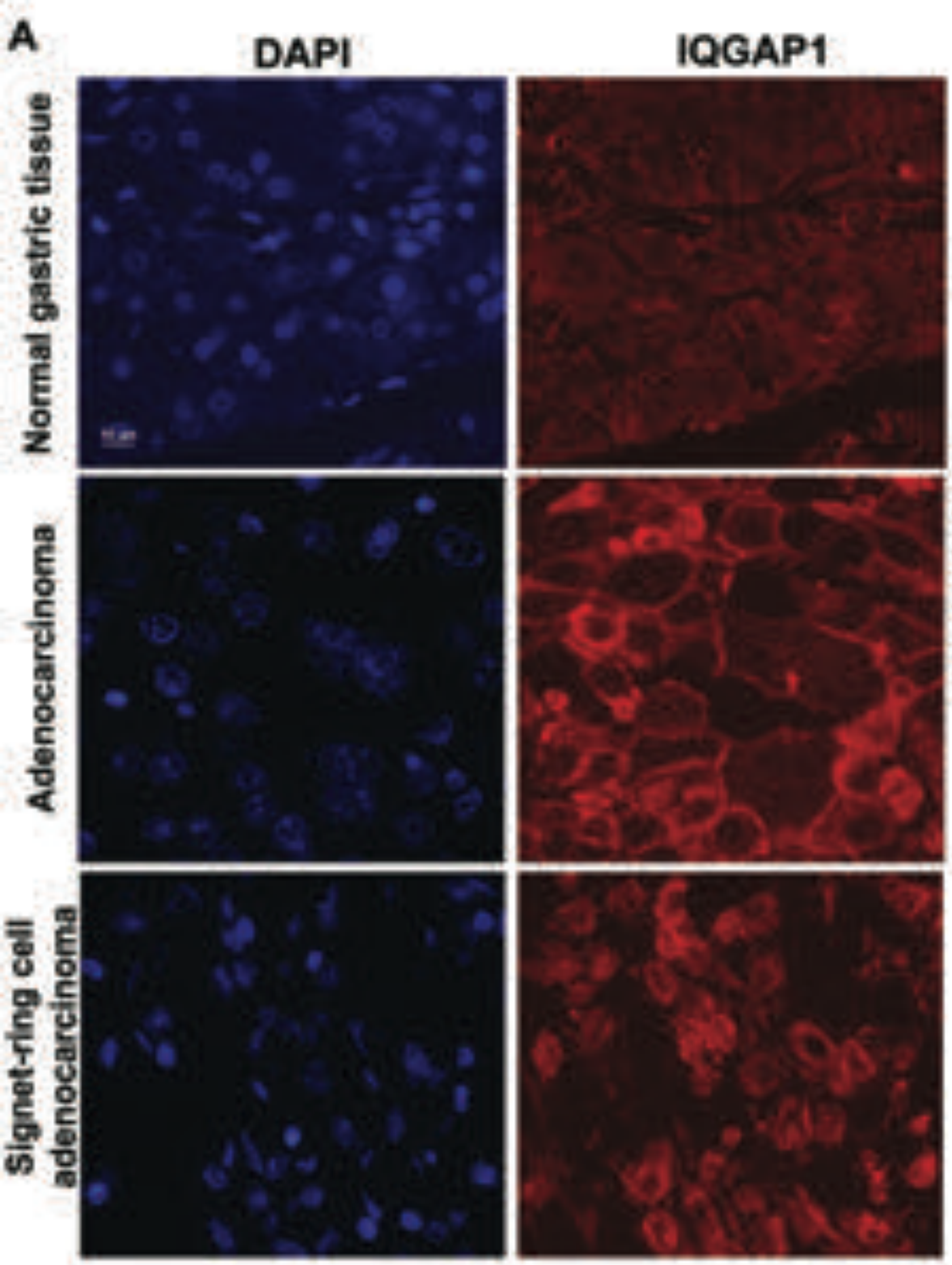
A
DAPI
IQGAP1
Normal gastric tissue
Adenocarcinoma
Signet-ring cell adenocarcinoma

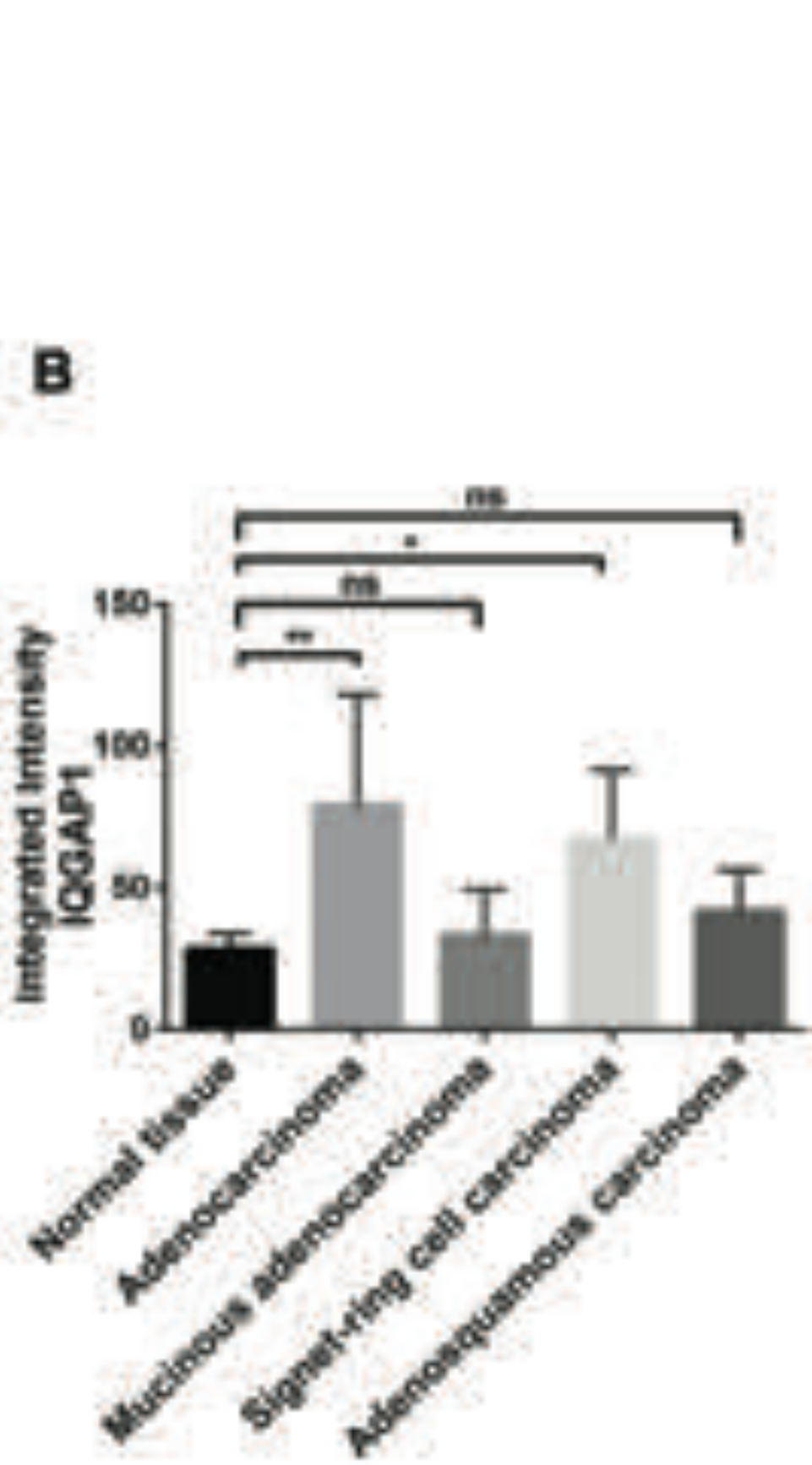
B
ns
*
ns
**
****
150
100
50
0
Integrated intensity of IQGAP1
Normal tissue
Adenocarcinoma
Mucinous adenocarcinoma
Signet-ring cell carcinoma
Adenosquamous carcinoma

C
TCGA STES
IQGAP1
TCGA STAD
IQGAP1
***
***
Distribution of gene expression
14
12
10
8
6
Tumor
Normal


D
AGS
MKN45
KATOIII
NUGC4
IQGAP1
β- actin
-190
-42
IQGAP1/β-actin
10
8
6
4
2
0
*
AGS
MKN45
KATOIII
NUGC4

Figure 1

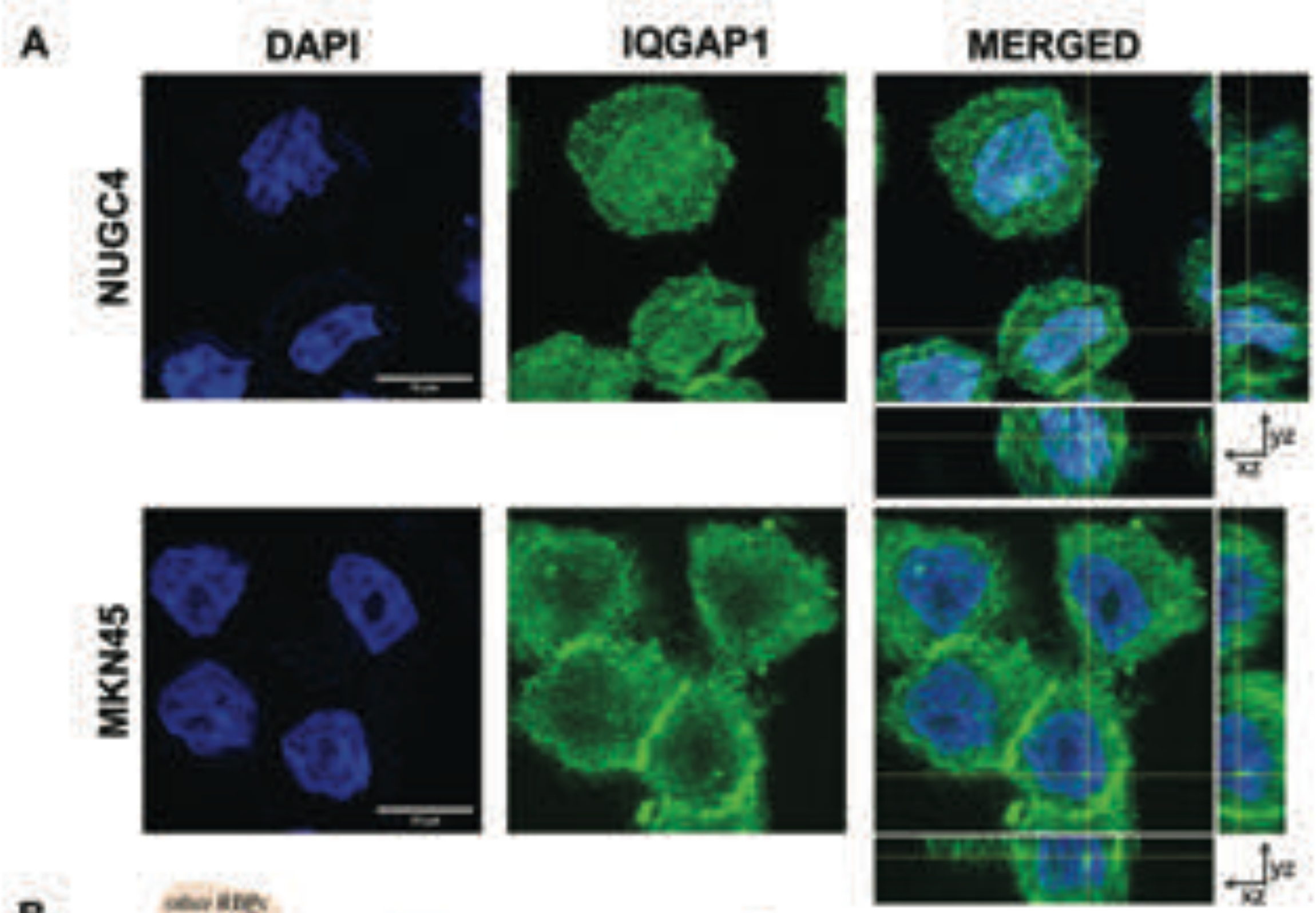
A
DAPI
IQGAP1
MERGED
NUGC4
MKN45
B
IQGAP1
C
NUGC4
MKN45
IP:
anti-IQGAP1
IgG
RNaseA:
input
IQGAP1
hnRNPA1
hnRNPL
hnRNPC1/C2
DHX9
hnRNPA2B1
hnRNPM
hnRNPM/IQGAP1
3.6 ±0.02
2.0 ±0.003
6.0 ±0.47
5.6 ±0.76

Figure 2

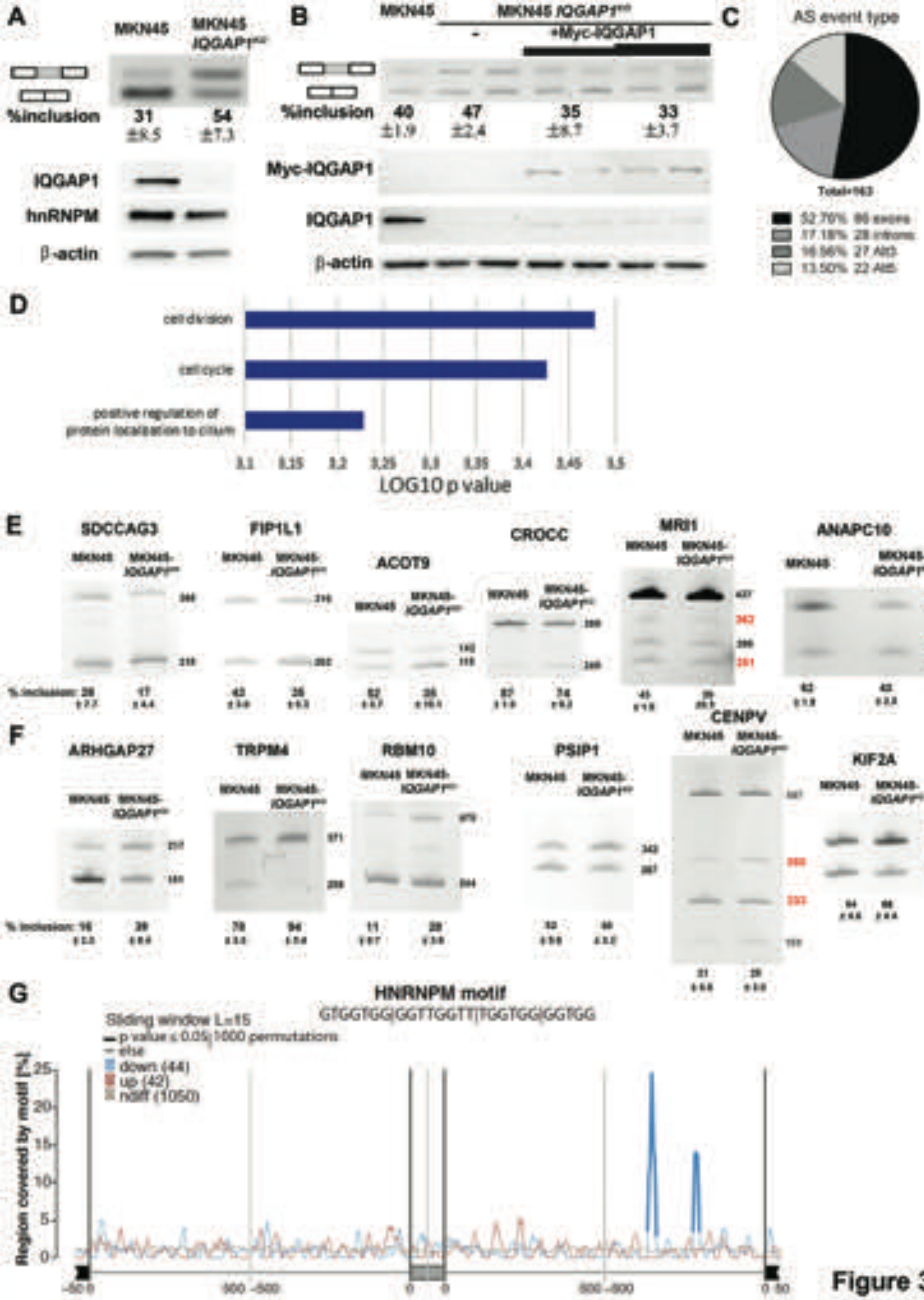
A
MKN45
MKN45 IQGAP1KO
%inclusion
31 ±8.5
54 ±7.3
IQGAP1
hnRNPM
β-actin
B
MKN45
MKN45 IQGAP1KO
-
+Myc-IQGAP1
%inclusion
40 ±1.9
47 ±2.4
35 ±6.7
33 ±3.7
Myc-IQGAP1
IQGAP1
β-actin
C
AS event type
Total=163
52.76% 86 exons
17.18% 28 introns
16.56% 27 Alt3
13.50% 22 Alt5
D
cell division
cell cycle
positive regulation of protein localization to cilium
LOG10 p value
E
SDCCAG3
FIP1L1
ACOT9
CROCC
MRI1
ANAPC10
MKN45
MKN45-IQGAP1KO
% inclusion:
F
ARHGAP27
TRPM4
RBM10
PSIP1
CENPV
KIF2A
G
HNRNPM motif
GTGGTGG|GGTTGGTT|TGGTGG|GGTGG
Sliding window L=15
p value ≤ 0.05, 1000 permutations
else
down (44)
up (42)
ndiff (1050)
Region covered by motif [%]

Figure 3

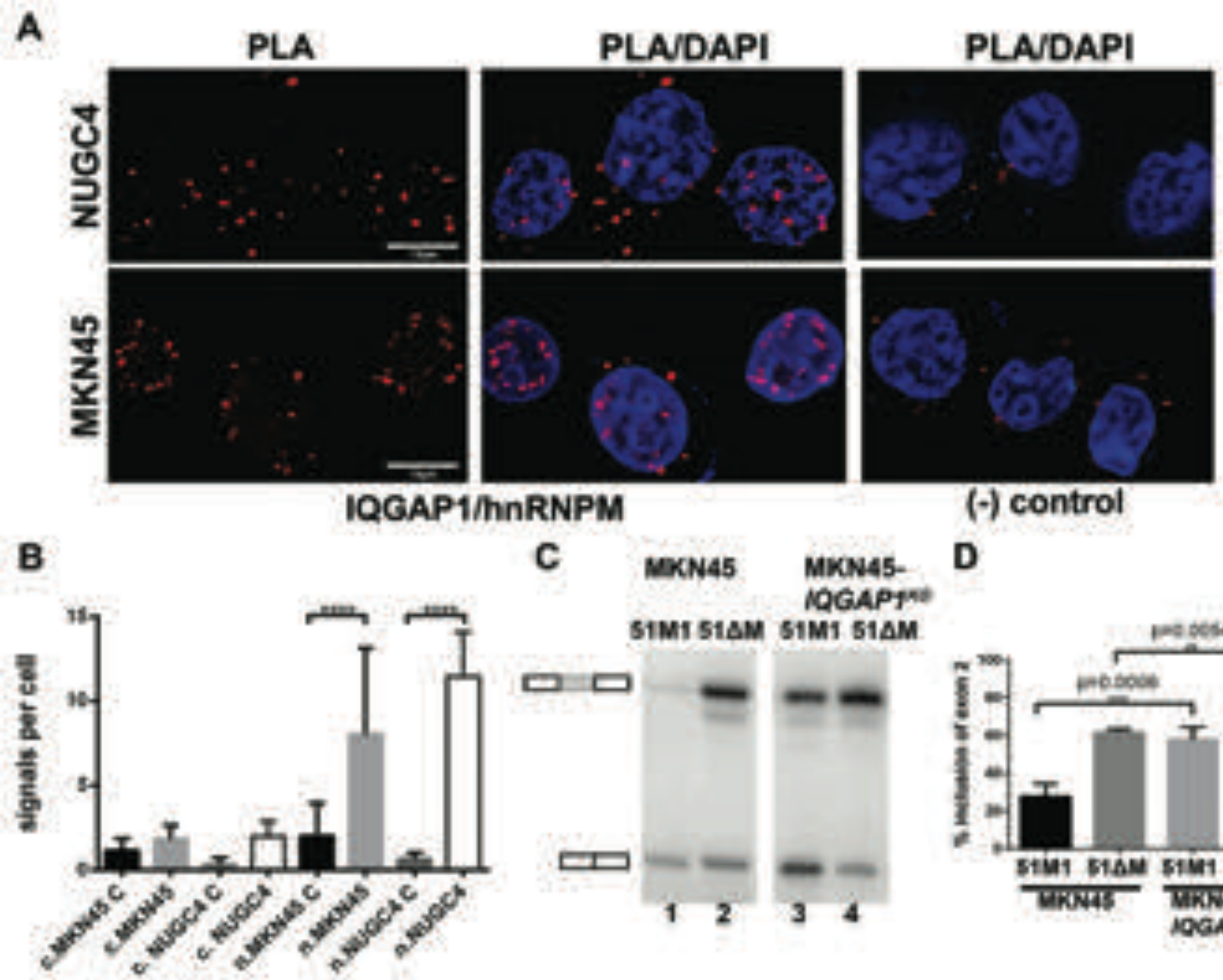
A
PLA
PLA/DAPI
PLA/DAPI
NUGC4
MKN45
IQGAP1/hnRNPM
(-) control
B
signals per cell
15
10
5
0
c.MKN45 C
c.MKN45
c.NUGC4 C
c.NUGC4
n.MKN45 C
n.MKN45
n.NUGC4 C
n.NUGC4
C
MKN45
MKN45-IQGAP1^KO
S1M1 S1ΔM S1M1 S1ΔM
1 2 3 4
D
% inclusion of exon 2
100
80
60
40
20
0
p=0.0054
p=0.0006
S1M1 S1ΔM S1M1 S1ΔM
MKN45
MKN45-IQGAP1^KO

Figure 4

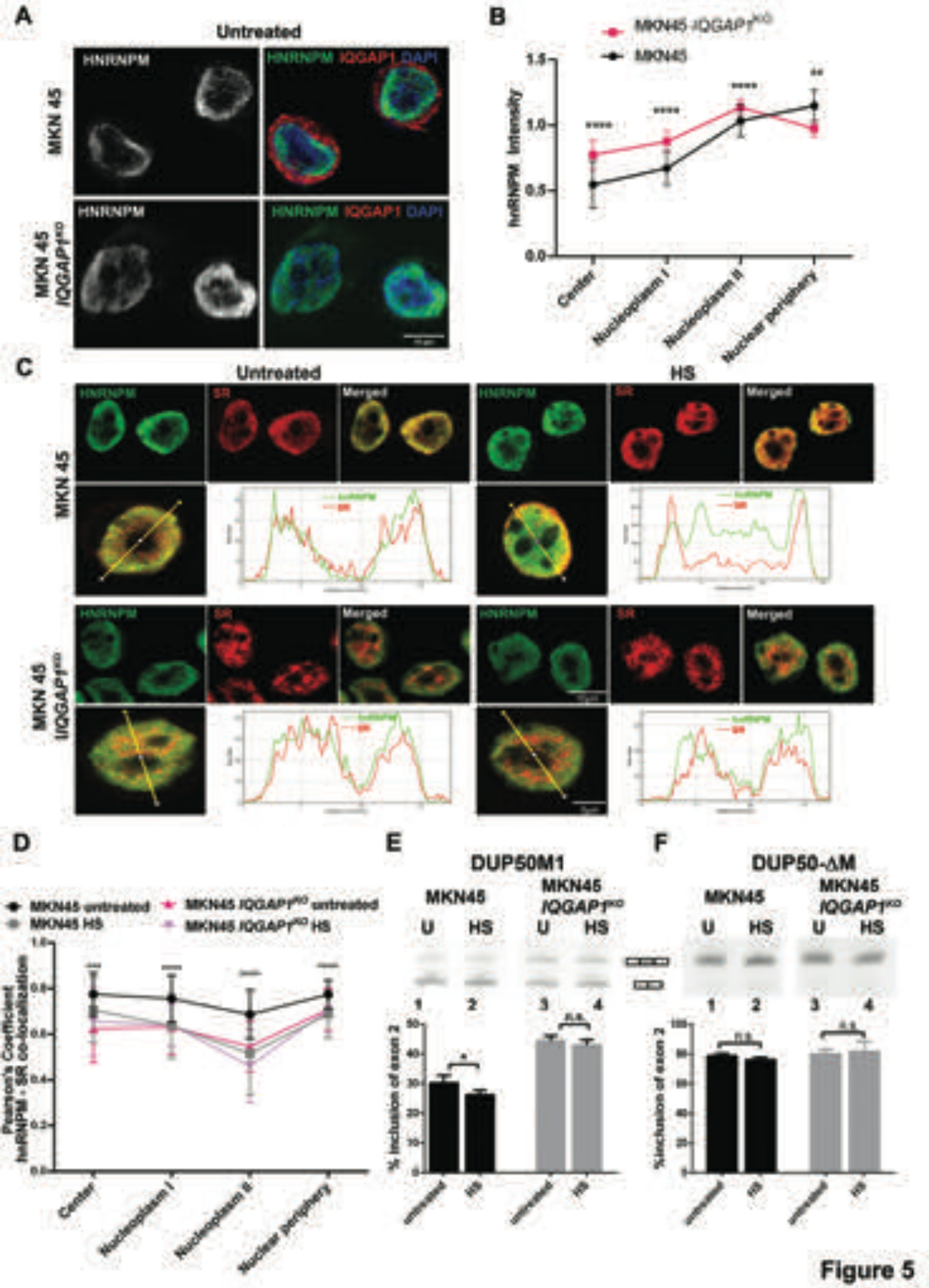
A
Untreated
HS
MKN 45
MKN 45 IQGAP1KO
HNRNPM
HNRNPM IQGAP1 DAPI
B
MKN45 IQGAP1KO
MKN45
hnRNPM Intensity
1.5
1.0
0.5
0.0
****
****
****
**
Center
Nucleoplasm I
Nucleoplasm II
Nucleus periphery
C
Untreated
HS
HNRNPM
SR
Merged
MKN 45
MKN 45 IQGAP1KO
D
MKN45 untreated
MKN45 HS
MKN45 IQGAP1KO untreated
MKN45 IQGAP1KO HS
Pearson's Coefficient hnRNPM - SR co-localization
Center
Nucleoplasm I
Nucleoplasm II
Nucleus periphery
E
DUP50M1
MKN45
MKN45 IQGAP1KO
U
HS
% inclusion of exon 2
F
DUP50-ΔM
MKN45
MKN45 IQGAP1KO
U
HS
% inclusion of exon 2

Figure 5

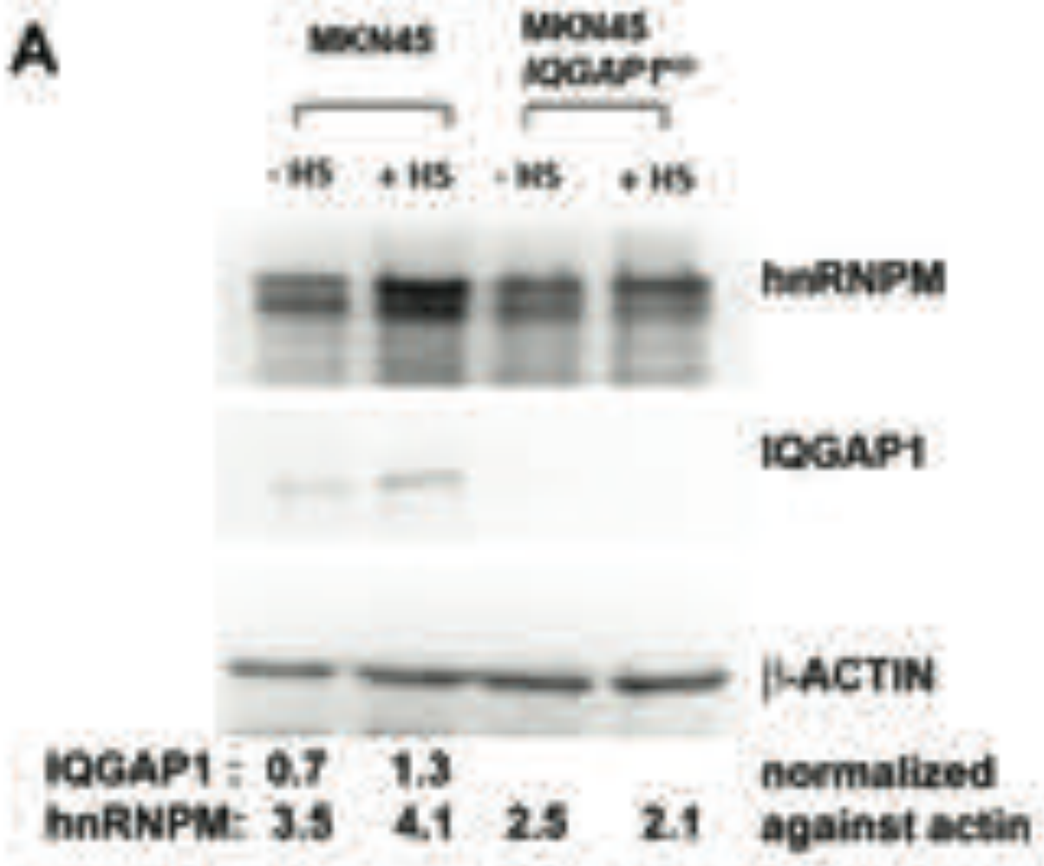
A
MKN45
MKN45 IQGAP1KD
- HS
+ HS
- HS
+ HS
hnRNPM
IQGAP1
β-ACTIN
IQGAP1 : 0.7 1.3
hnRNPM: 3.5 4.1 2.5 2.1
normalized against actin

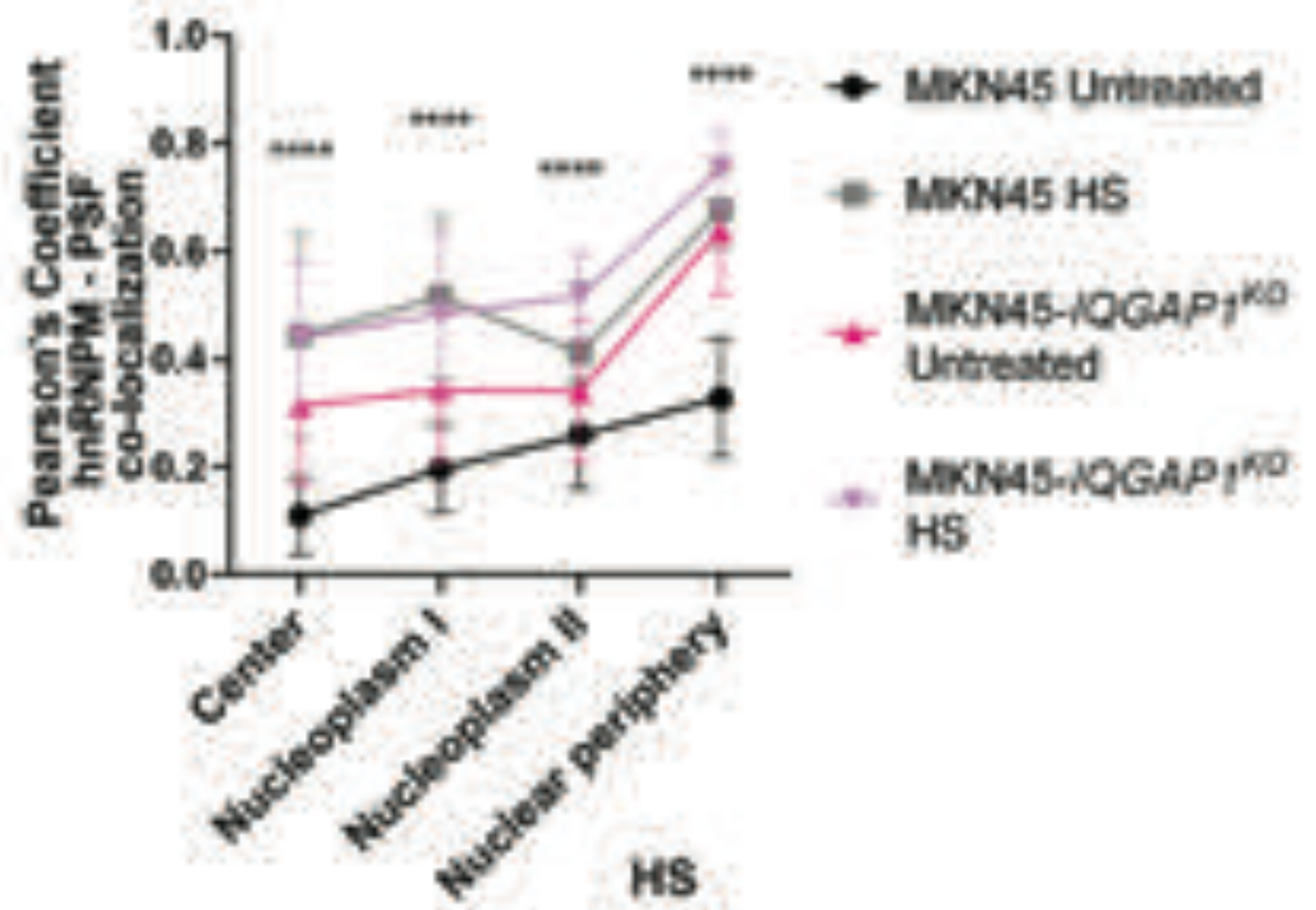
C
Pearson's Coefficient hnRNPM - PSF co-localization
1.0
0.8
0.6
0.4
0.2
0.0
****
****
****
****
Center
Nucleoplasm I
Nucleoplasm II
Nuclear periphery
MKN45 Untreated
MKN45 HS
MKN45-IQGAP1KD Untreated
MKN45-IQGAP1KD HS

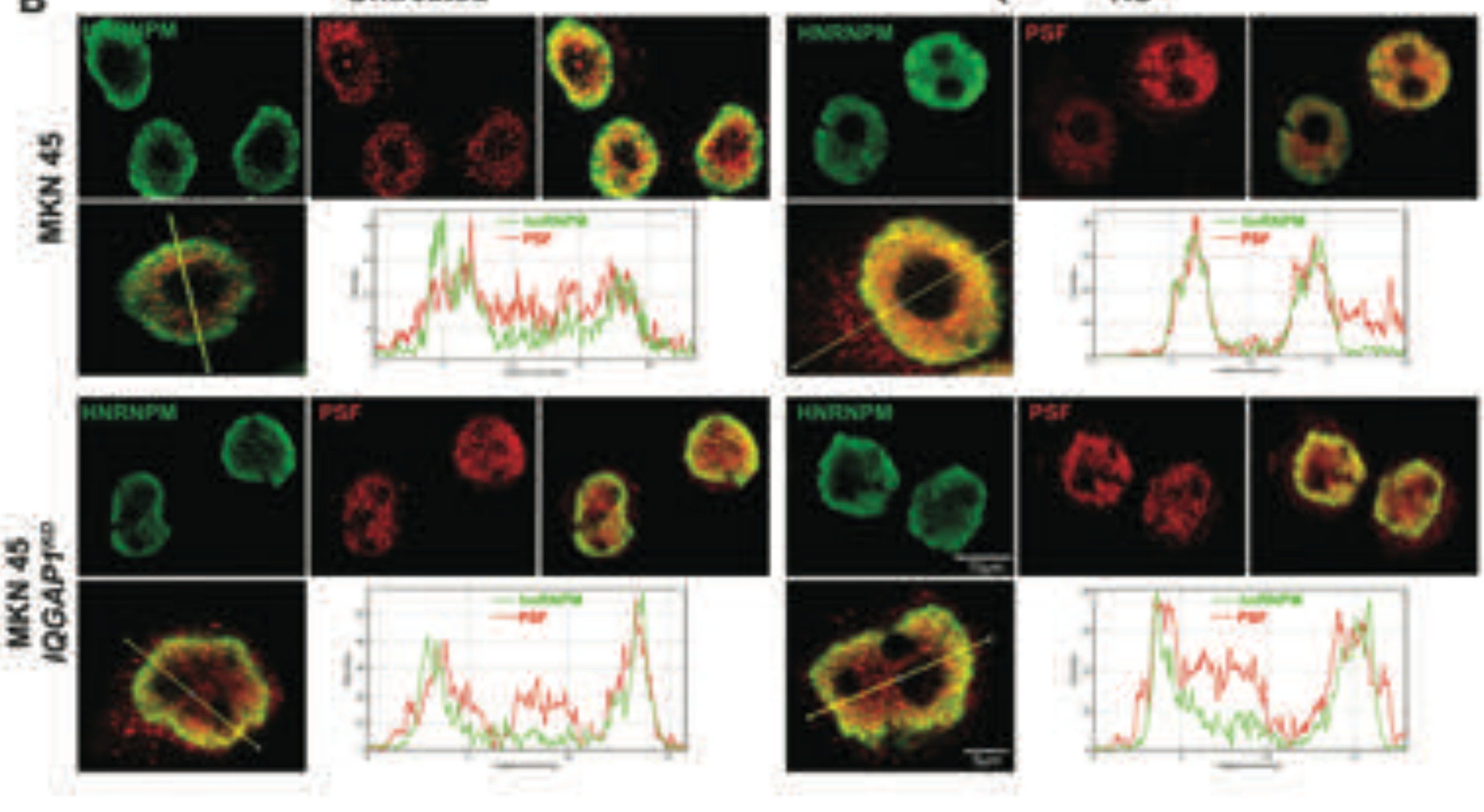
B
Untreated
HS
MKN 45
MKN 45 IQGAP1KD
HNRNPM
PSF
IQGAP1
PSF

Figure 6

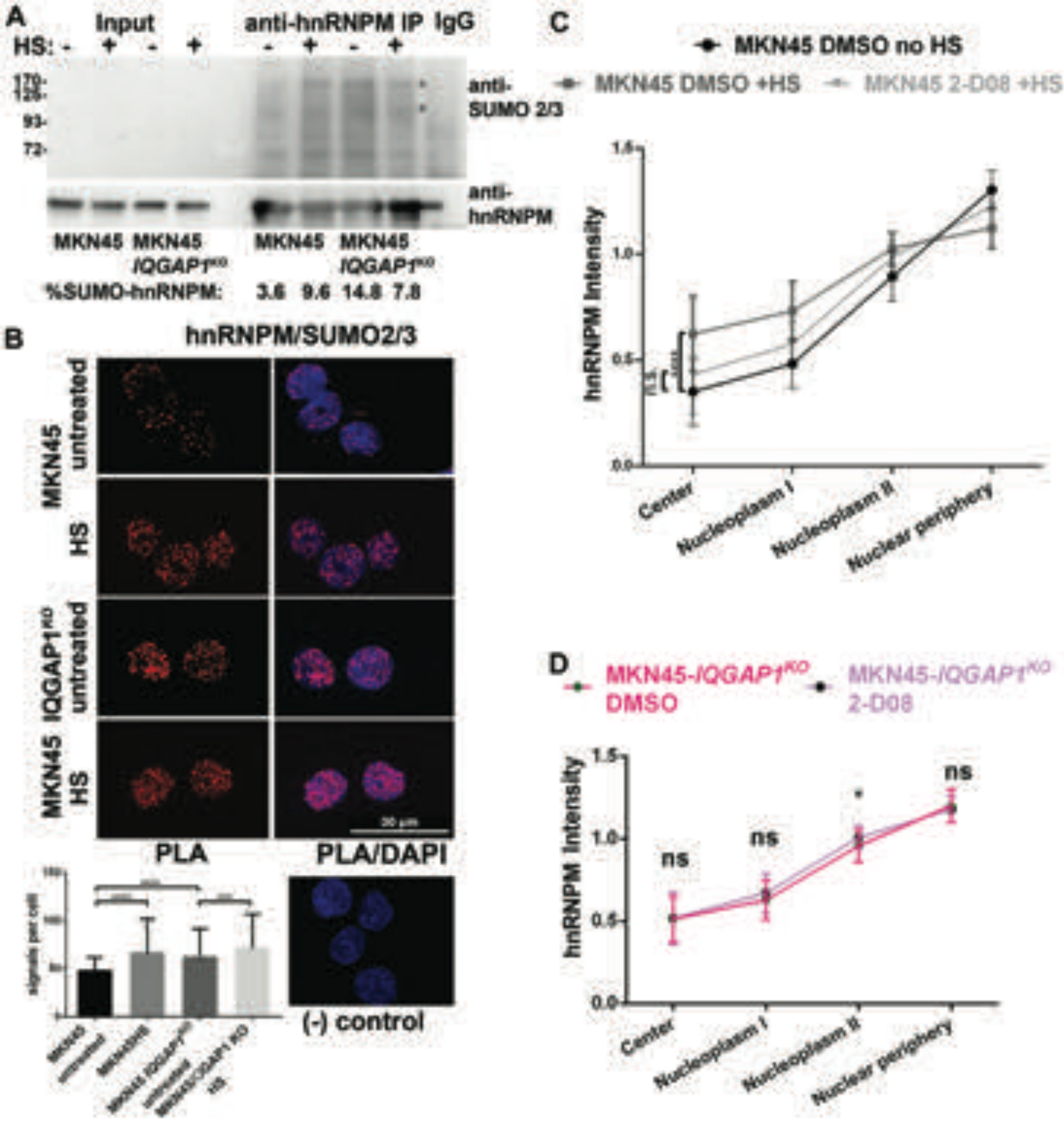
A
Input
anti-hnRNPM IP
IgG
HS: - + - + - + - +
170-
130-
93-
72-
anti-SUMO 2/3
anti-hnRNPM
MKN45
MKN45 /IQGAP1KO
MKN45
MKN45 /IQGAP1KO
%SUMO-hnRNPM: 3.6 9.6 14.8 7.8
B
hnRNPM/SUMO2/3
MKN45 untreated
HS
IQGAP1KO untreated
HS
30 µm
PLA
PLA/DAPI
(-) control
C
MKN45 DMSO no HS
MKN45 DMSO +HS
MKN45 2-D08 +HS
hnRNPM Intensity
1.5
1.0
0.5
0.0
Center
Nucleoplasm I
Nucleoplasm II
Nuclear periphery
D
MKN45-IQGAP1KO DMSO
MKN45-IQGAP1KO 2-D08
hnRNPM Intensity
ns
ns
*
ns
Center
Nucleoplasm I
Nucleoplasm II
Nuclear periphery

Figure 7

A

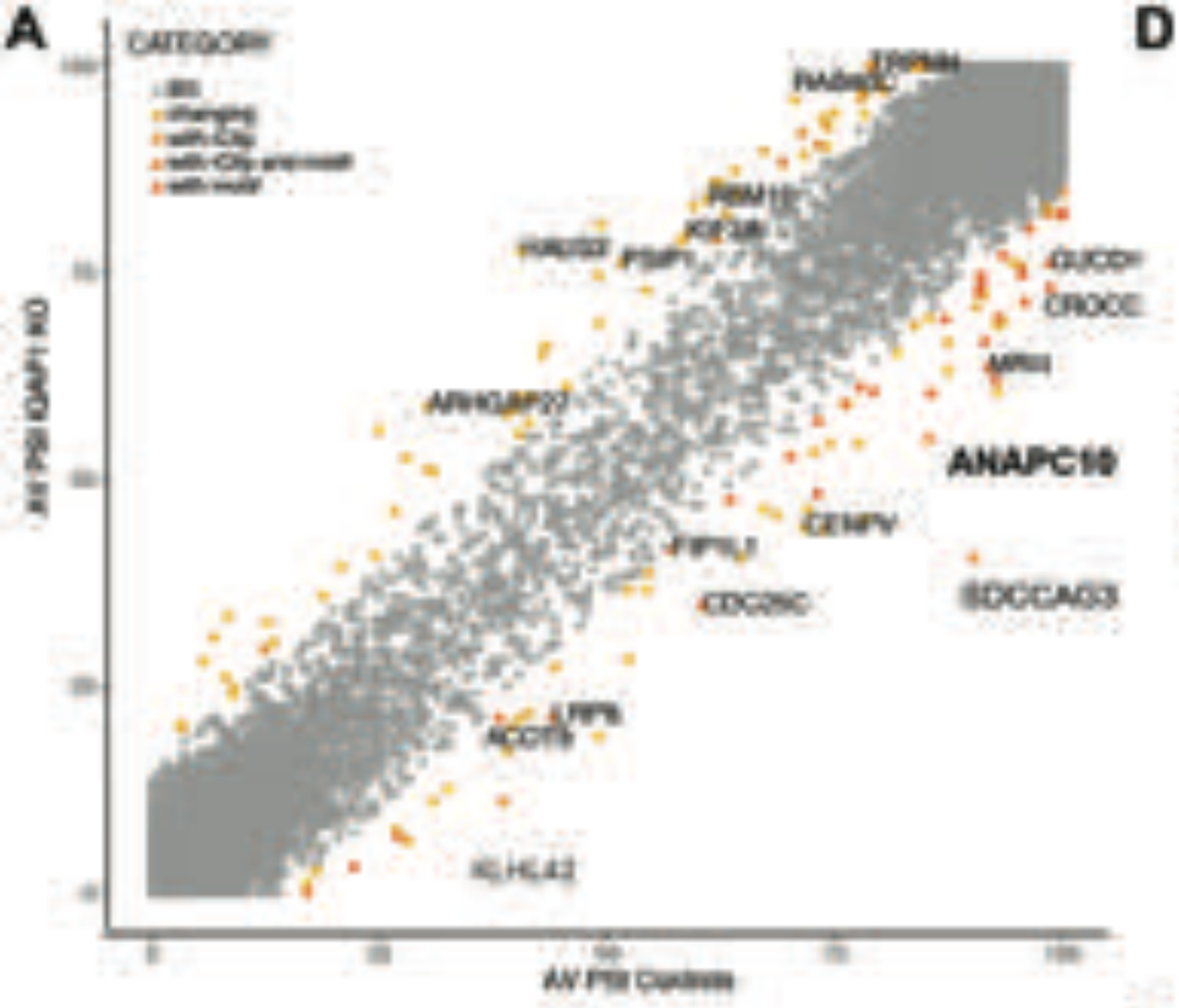

B

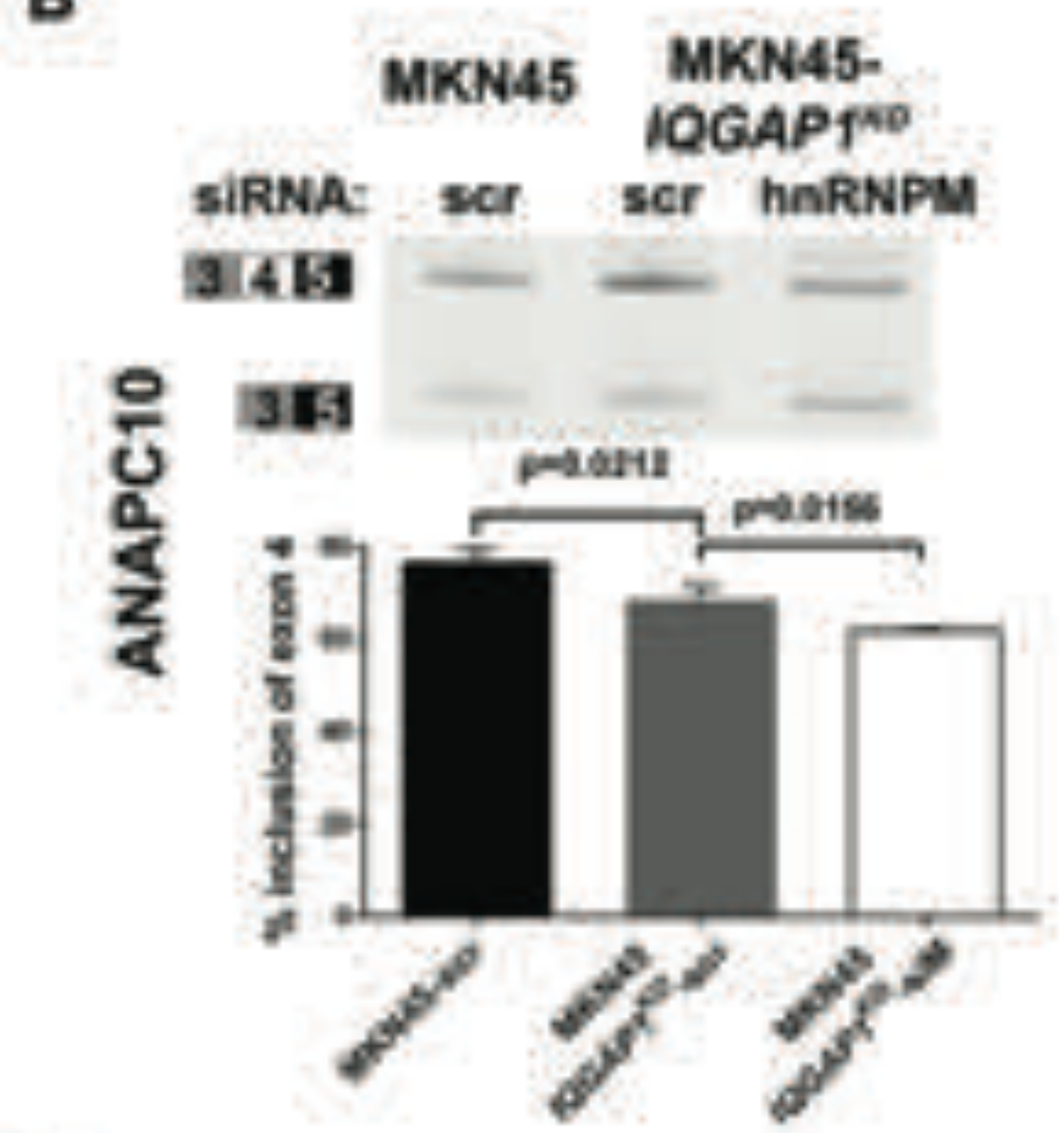

C

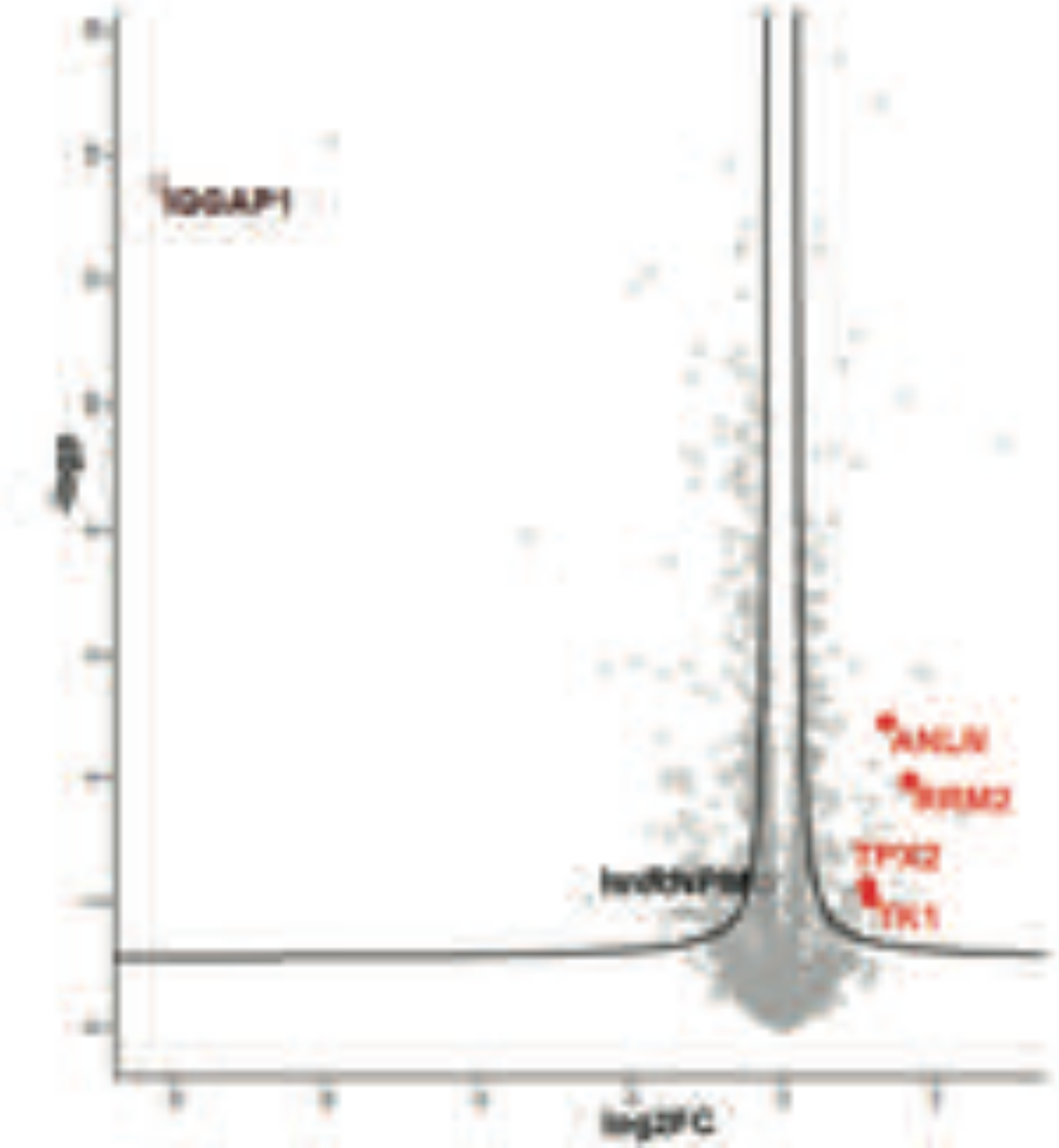

D

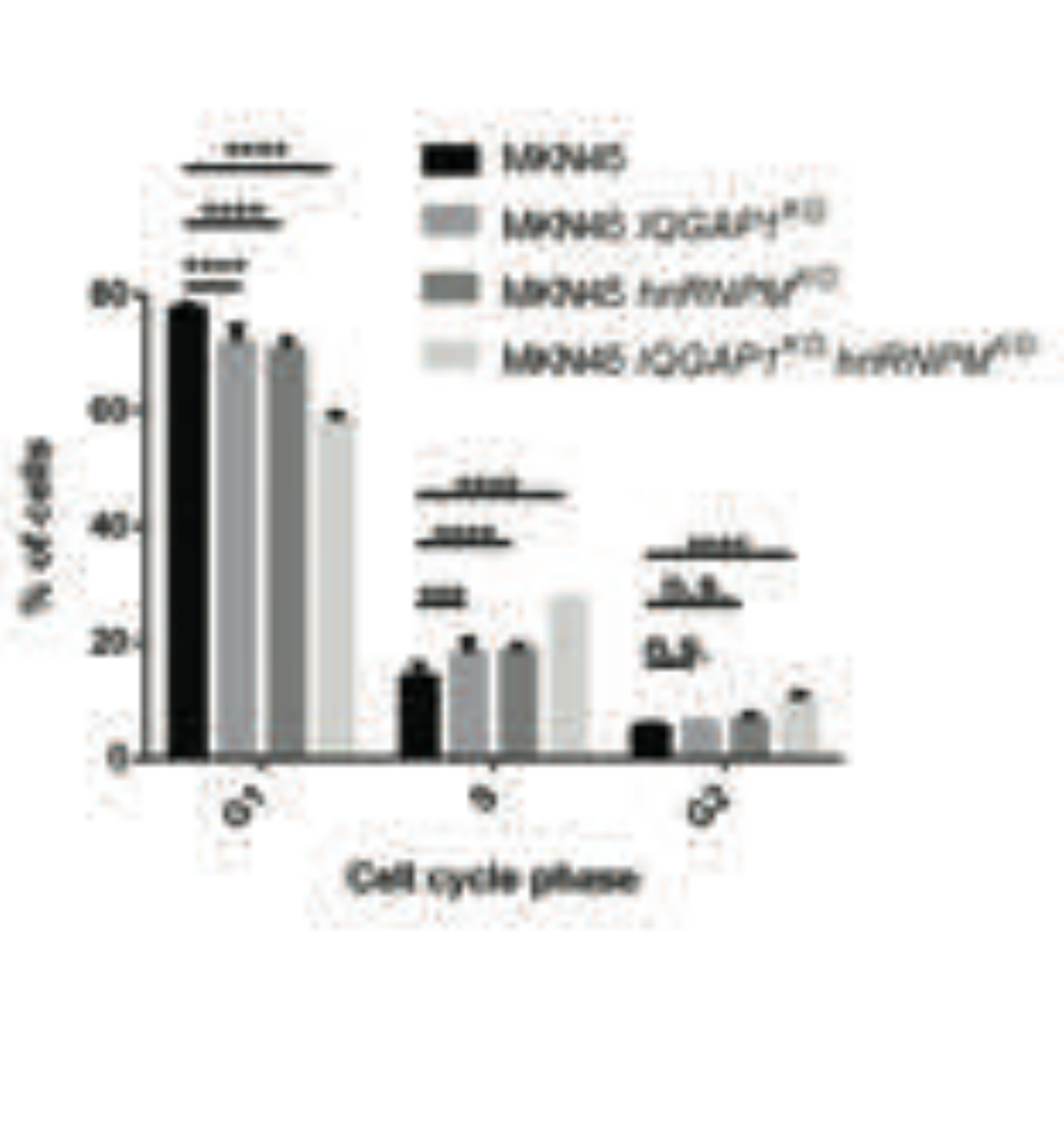

E

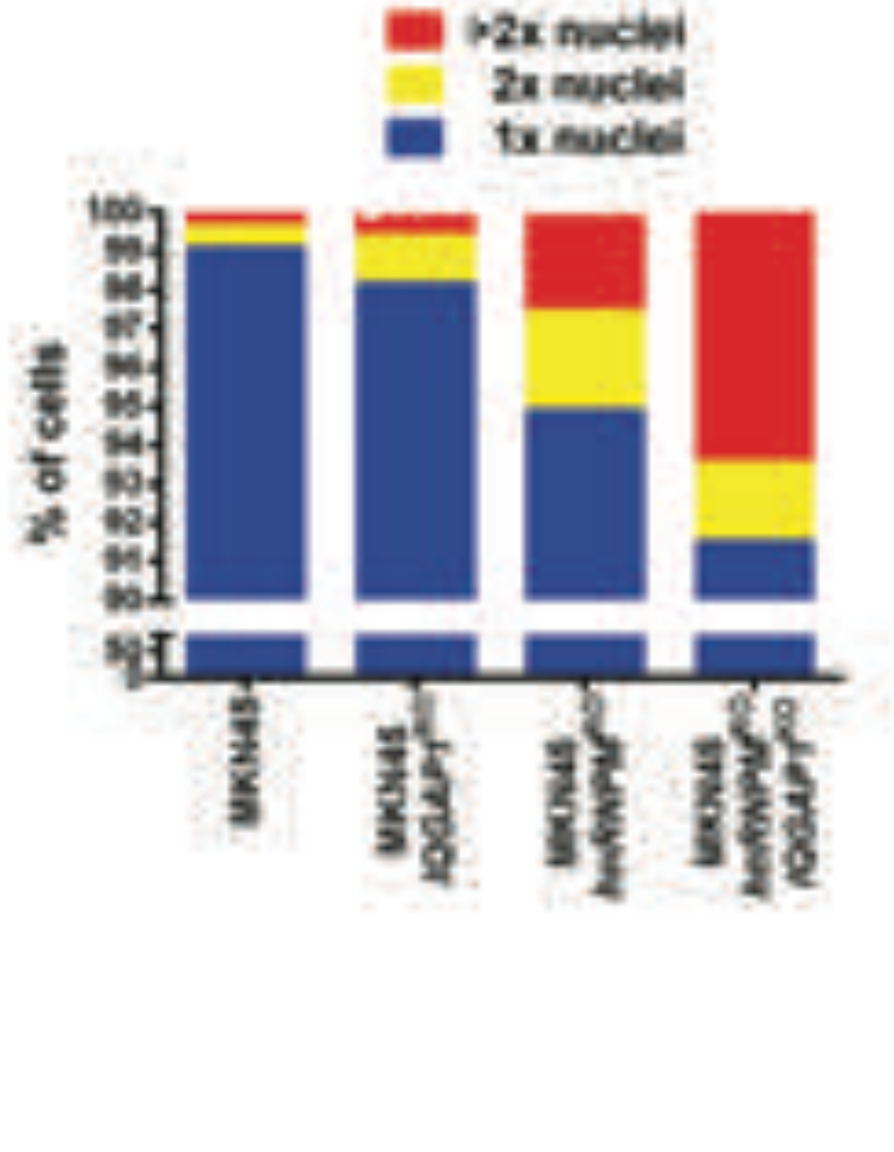

F

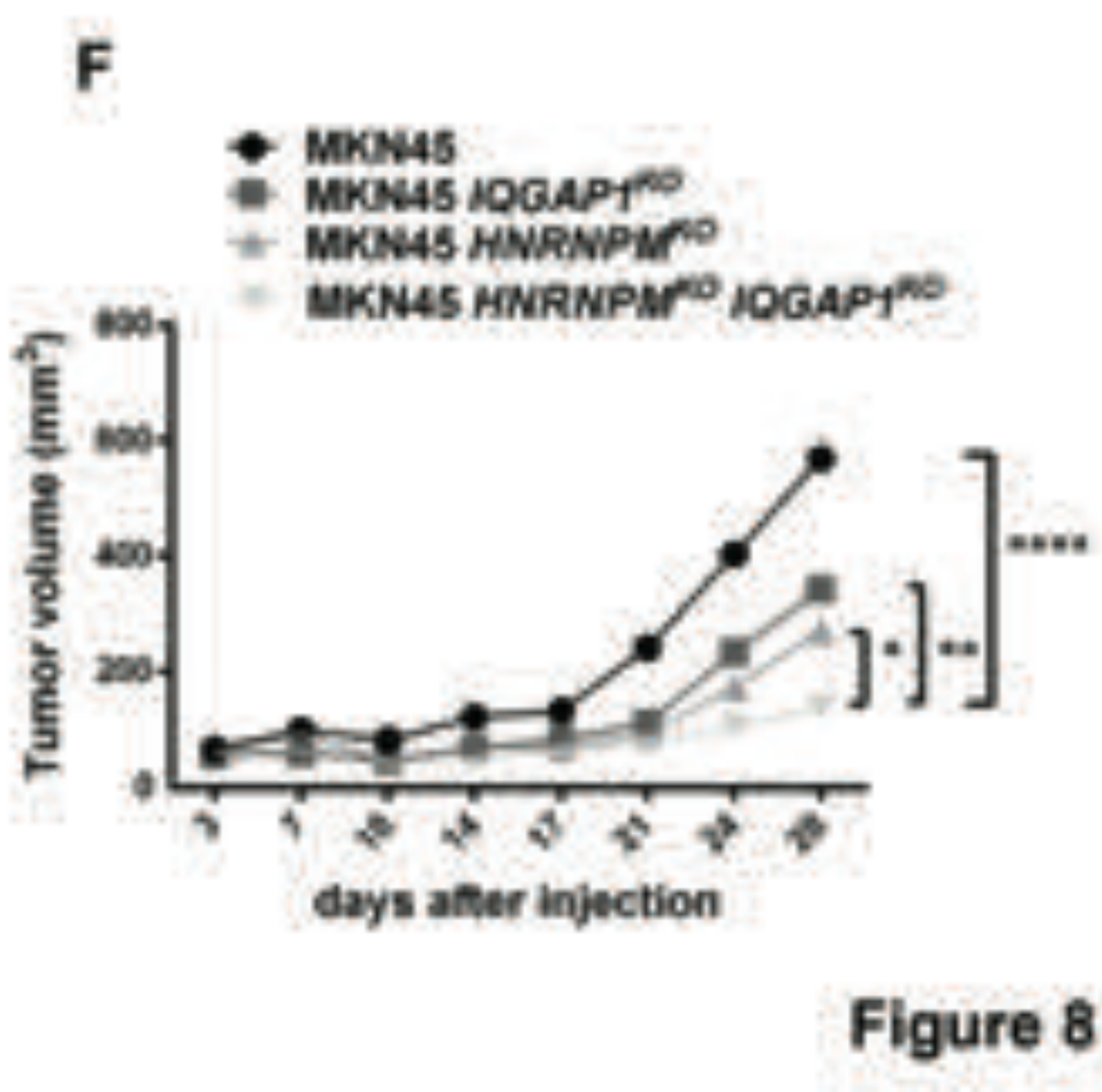

Figure 8